Article

Cell

Distinct Hippocampal Pathways Mediate Dissociable Roles of Context in Memory Retrieval

Graphical Abstract

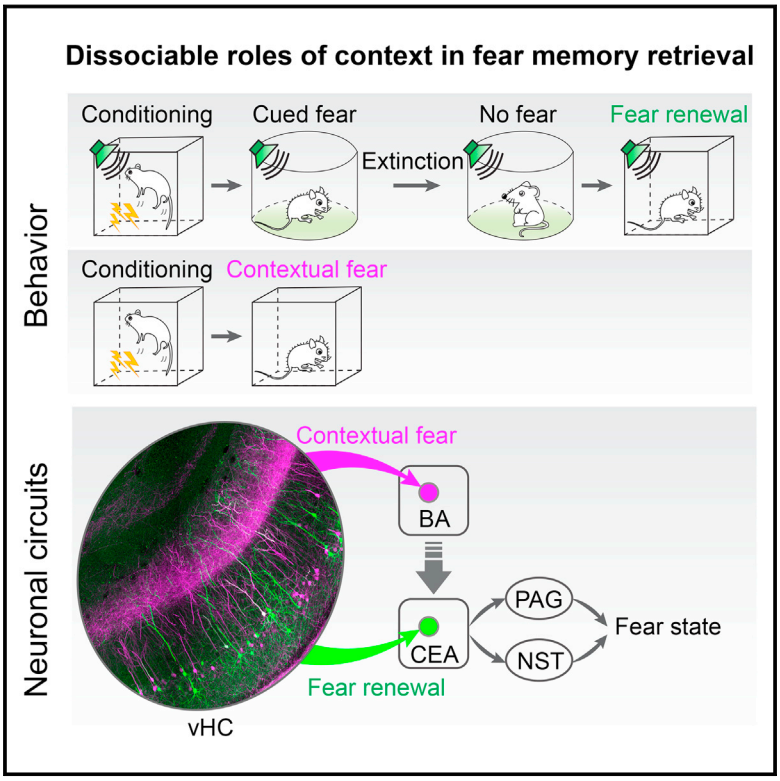

Authors

Chun Xu, Sabine Krabbe, Jan Gründemann, ..., Mark J. Schnitzer, Edward M. Callaway, Andreas Lüthi

Correspondence

andreas.luthi@fmi.ch

In Brief

Two parallel hippocampal circuits link sensory memories with the context in which they are formed, helping the selection of appropriate behavioral responses to fear.

Highlights

- vHC projects to the BA and the CEA via separate pathways with distinct behavioral roles
- vHC inputs to the CEA contact output cells that target PAG and NST
- vHC projection to the BA is required for contextual fear memory retrieval
- vHC projection to the CEA is necessary for context-dependent cue fear memory retrieval

Xu et al., 2016, Cell *167*, 961–972
November 3, 2016
http://dx.doi.org/10.1016/j.cell.2016.09.051

CellPress

Article

Cell

Distinct Hippocampal Pathways Mediate Dissociable Roles of Context in Memory Retrieval

Chun Xu,[1] Sabine Krabbe,[1] Jan Gründemann,[1] Paolo Botta,[1,2,7] Jonathan P. Fadok,[1] Fumitaka Osakada,[3,8] Dieter Saur,[4,5] Benjamin F. Grewe,[6] Mark J. Schnitzer,[6] Edward M. Callaway,[3] and Andreas Lüthi[1,2,9,*]

[1]Friedrich Miescher Institute for Biomedical Research, Maulbeerstrasse 66, 4058 Basel, Switzerland
[2]University of Basel, 4003 Basel, Switzerland
[3]Systems Neurobiology Laboratories, Salk Institute for Biological Studies, La Jolla, CA 92037, USA
[4]Department of Internal Medicine 2, Technische Universität München, Ismaningerstrasse 22, 81675 Munich, Germany
[5]German Cancer Consortium (DKTK) and German Cancer Research Center (DKFZ), Im Neuenheimer Feld 280, 69120 Heidelberg, Germany
[6]CNC Program, Howard Hughes Medical Institute, Stanford University, Stanford, CA 94305, USA
[7]Present address: Champalimaud Neuroscience Programme, Fundação Champalimaud, 1400-038 Lisbon, Portugal
[8]Present address: Laboratory of Cellular Pharmacology, Nagoya University, Nagoya 464-8601, Japan
[9]Lead Contact
*Correspondence: andreas.luthi@fmi.ch
http://dx.doi.org/10.1016/j.cell.2016.09.051

SUMMARY

Memories about sensory experiences are tightly linked to the context in which they were formed. Memory contextualization is fundamental for the selection of appropriate behavioral reactions needed for survival, yet the underlying neuronal circuits are poorly understood. By combining *trans*-synaptic viral tracing and optogenetic manipulation, we found that the ventral hippocampus (vHC) and the amygdala, two key brain structures encoding context and emotional experiences, interact via multiple parallel pathways. A projection from the vHC to the basal amygdala mediates fear behavior elicited by a conditioned context, whereas a parallel projection from a distinct subset of vHC neurons onto midbrain-projecting neurons in the central amygdala is necessary for context-dependent retrieval of cued fear memories. Our findings demonstrate that two fundamentally distinct roles of context in fear memory retrieval are processed by distinct vHC output pathways, thereby allowing for the formation of robust contextual fear memories while preserving context-dependent behavioral flexibility.

INTRODUCTION

Classical auditory fear conditioning is one of the most powerful behavioral models used to study the fundamental principles of associative learning and the underlying neuronal mechanisms (Davis, 2000; Fanselow and Poulos, 2005; LeDoux, 2000; Maren, 2001). In classical auditory fear conditioning, an auditory cue, the so-called conditioned stimulus (CS), is associated with an aversive shock, the unconditioned stimulus (US). Upon re-exposure to the CS a fear response is elicited consisting of defensive behavior, such as freezing or flight, as well as autonomic, neuroendocrine, and other components (Davis, 1992; Kapp et al., 1979; LeDoux et al., 1988). During auditory fear conditioning, not only the auditory cue becomes associated with the US, but also the context in which conditioning occurs (LeDoux, 2000; Maren, 2001). Consequently, animals will show a fear reaction to both the conditioning context as well as to the auditory CS. Nevertheless, the initial CS-US association can be retrieved in a context-independent manner (Tovote et al., 2015). Interestingly, subsequent extinction or counter-conditioning of the CS renders CS memory retrieval highly context-dependent (Bouton, 2004; Maren et al., 2013; Maren and Quirk, 2004). This indicates that context can not only be directly associated with the US, thereby acting as a complex cue consisting of a set of external and internal sensory stimuli, but that it can also act as a so-called "occasion setter" that modulates the retrieval of discrete CS-US associations in a context-dependent manner (Bouton and Swartzentruber, 1986). Behavioral experiments indicate that these two fundamentally different roles of context can be manipulated independently, but, nevertheless, interact (Urcelay and Miller, 2014). This raises the question of whether context-US associations and context-dependent occasion setting are mediated by functionally dedicated and anatomically distinct neuronal circuits.

The amygdala plays a central role in the acquisition and expression of conditioned fear responses to both auditory CSs and context (LeDoux, 2000; Maren, 2001). Anatomically, the amygdala can be divided into the basolateral amygdala (BLA), consisting of the lateral (LA), basal (BA), and basomedial (BMA) nuclei, and the central amygdala (CEA), consisting of a lateral (CEl) and medial (CEm) subdivision (Pitkänen et al., 1997; Swanson and Petrovich, 1998). The BLA receives direct cortical and thalamic sensory inputs and is reciprocally connected with many forebrain structures including the medial prefrontal cortex (mPFC) and the hippocampus (Pitkänen et al., 2000). The CEA projects to the hypothalamic and midbrain structures involved in the expression of conditioned fear responses (Gross and Canteras, 2012; Petrovich et al., 2001; Veening et al., 1984).

The hippocampus processes contextual information and is required for both contextual fear conditioning as well as for the contextual gating of cued fear memory retrieval (Hobin et al.,

2006; Ji and Maren, 2007; Kim and Fanselow, 1992; Phillips and LeDoux, 1992). The ventral hippocampus (vHC) strongly projects to the BA, which sends reciprocal connections back to the vHC (Petrovich et al., 2001; Pitkänen et al., 2000). Based on lesion studies, it has been postulated that vHC inputs to the BA, together with a largely separate projection to the mPFC (Lee et al., 2014), underlie the contextual modulation of cued fear memory retrieval (e.g., fear renewal after extinction) (Orsini et al., 2011).

In addition to the reciprocal connections with the BA and the BMA, the vHC also sends a weaker projection to the CEA (Cenquizca and Swanson, 2007; Kishi et al., 2006). Given that CEA output neurons project directly to midbrain structures, such as the periaqueductal gray (PAG) (LeDoux et al., 1988), controlling fear behavior, the vHC→CEA pathway would be in an ideal position to mediate contextual gating of cued fear memory retrieval. That is, during cued fear memory retrieval, vHC could directly impinge onto CEA output mediating CS-induced fear responses and thereby integrate contextual information into cued fear expression. However, because of technical limitations, the behavioral function of this pathway has not been addressed to date.

In the present study, by combining rabies virus-mediated *trans*-synaptic circuit tracing with optogenetic manipulations, we found a functional double-dissociation between the vHC projections targeting the CEA and the BA. We demonstrate that the vHC→CEA pathway is required for contextual gating of cued fear memory retrieval by means of excitatory connections onto midbrain-projecting CEA output neurons. In contrast, the vHC→BA pathway is necessary for the retrieval of contextual fear memories, but not for the gating of CS fear memory retrieval. Our study uncovers an unexpected pathway specificity of hippocampus-amygdala circuitry underlying distinct aspects of contextual regulation of fear behavior.

RESULTS

The vHC Projects onto CEA Output Neurons

The CEA mediates fear-induced freezing responses through a strong projection to the ventrolateral PAG (vlPAG) (Gross and Canteras, 2012; LeDoux, 2000). To investigate whether vHC directly projects onto vlPAG-targeting CEA output neurons, we adapted a *trans*-synaptic circuit-tracing strategy using a rabies virus strain (rabiesΔG) deficient for the rabies envelope glycoprotein (rabG) in adult C57BL/6 mice (Wickersham et al., 2007). To exclude a possible confound due to direct projections from the vHC to the vlPAG, we first performed direct retrograde tracing of long-range inputs to the vlPAG by infecting axon terminals with rabiesΔG-mCherry without complementation with rabG (Figures 1A–1D). Many retrogradely labeled vlPAG-projecting neurons were found in the CEA (rabies-labeled cells are shown in green in all figures for consistency), but also in other brain areas (Figures 1B and S1A). In contrast, no retrogradely labeled cells could be detected in the vHC (Figure 1E), confirming that the vHC does not directly project to the vlPAG. Next, we used an intersectional viral strategy to locally complement rabiesΔG-mCherry with rabG in the CEA, allowing rabies virus to jump across one synaptic connection, thereby specifically labeling neurons presynaptic to vlPAG-projecting CEA neurons (Figure 1F). A mixture of a retrogradely transported viral vector expressing Cre-recombinase (replication incompetent herpes simplex virus 1; HSV-Cre-Venus) and rabiesΔG-mCherry was injected into the vlPAG (Figures 1G–1I). For complementation with rabG, we locally injected into the CEA a conditional adeno-associated viral vector expressing rabG in a Cre-dependent manner (AAV-DIO-G). Using this approach, we found many *trans*-synaptically labeled neurons in the vHC (599 ± 110 neurons, n = 8 animals; Figures 1N and S1E), but also in BLA and in adjacent striatal areas (Figure S1F). When one of the three viral vectors (HSV-Cre-Venus, AAV-DIO-G, rabiesΔG-mCherry) was omitted, no labeled cells could be detected in the vHC (Figure S1B–S1D). Cells in the CEA that co-stained for rabiesΔG-mCherry and rabG were identified as starter cells (total starter cell number: 21 ± 6, n = 5 animals with immunostaining of rabG; Figures 1J–1M and S1G), which indicates that individual CEA output neurons receive converging input from a larger number of vHC neurons (convergence index: 32.4 ± 7.3, n = 5; number of vHC neurons/number of CEA starter neurons). The rabies-labeled vHC neurons were almost exclusively located on the ipsilateral side of the CEA starter cells (99.6% ± 0.08%, n = 6). Finally, rabies-labeled vHC neurons were mostly glutamatergic, as indicated by immunostaining against calcium/calmodulin-dependent protein kinase II (CaMKII) and gamma-aminobutyric acid (GABA) (CaMKII positive: 91.7% ± 4.8%, n = 3 animals; GABA positive: 0% ± 0%, n = 8 animals; Figure S1H). These results indicate that vHC sends a direct glutamatergic projection onto vlPAG-targeting CEA output neurons.

CEA output neurons project to multiple downstream target structures involved in distinct aspects of a fear response (Krettek and Price, 1978; Petrovich et al., 2001; Veening et al., 1984). Whereas projections to the vlPAG mediate conditioned freezing behavior, projections to the nucleus of the solitary tract (NST) regulate cardiovascular function (Dampney, 1994). To address whether vHC not only connects onto vlPAG-projecting CEA output neurons, we *trans*-synaptically labeled neurons presynaptic to NST-projecting CEA neurons and found a similar number of labeled vHC neurons (total cell number: 540 ± 98, n = 5 animals; Figures 2A–2G).

Notably, when separately injecting HSV-Cre-Venus into NST, rabiesΔG-mCherry into the vlPAG, and AAV-DIO-G into the CEA, we observed similar labeling of presynaptic neurons in vHC (total cell number in vHC: 380 ± 148, n = 3; Figures 2H–2S). Given that Cre recombinase is required in rabies-infected neurons for *trans*-synaptic labeling of presynaptic neurons, this indicates that CEA output neurons that receive vHC input can project to both the vlPAG and the NST. Taken together, these results suggest that the vHC could gate the context-dependent retrieval and expression of multiple components of a fear response through its direct projections onto CEA output neurons.

The vHC to CEA Pathway Is Monosynaptic and Excitatory

We next examined the synaptic function of vHC inputs to the CEA. We first expressed channelrhodopsin-2 (ChR2) in CEA-projecting vHC neurons by injecting a retrogradely transported

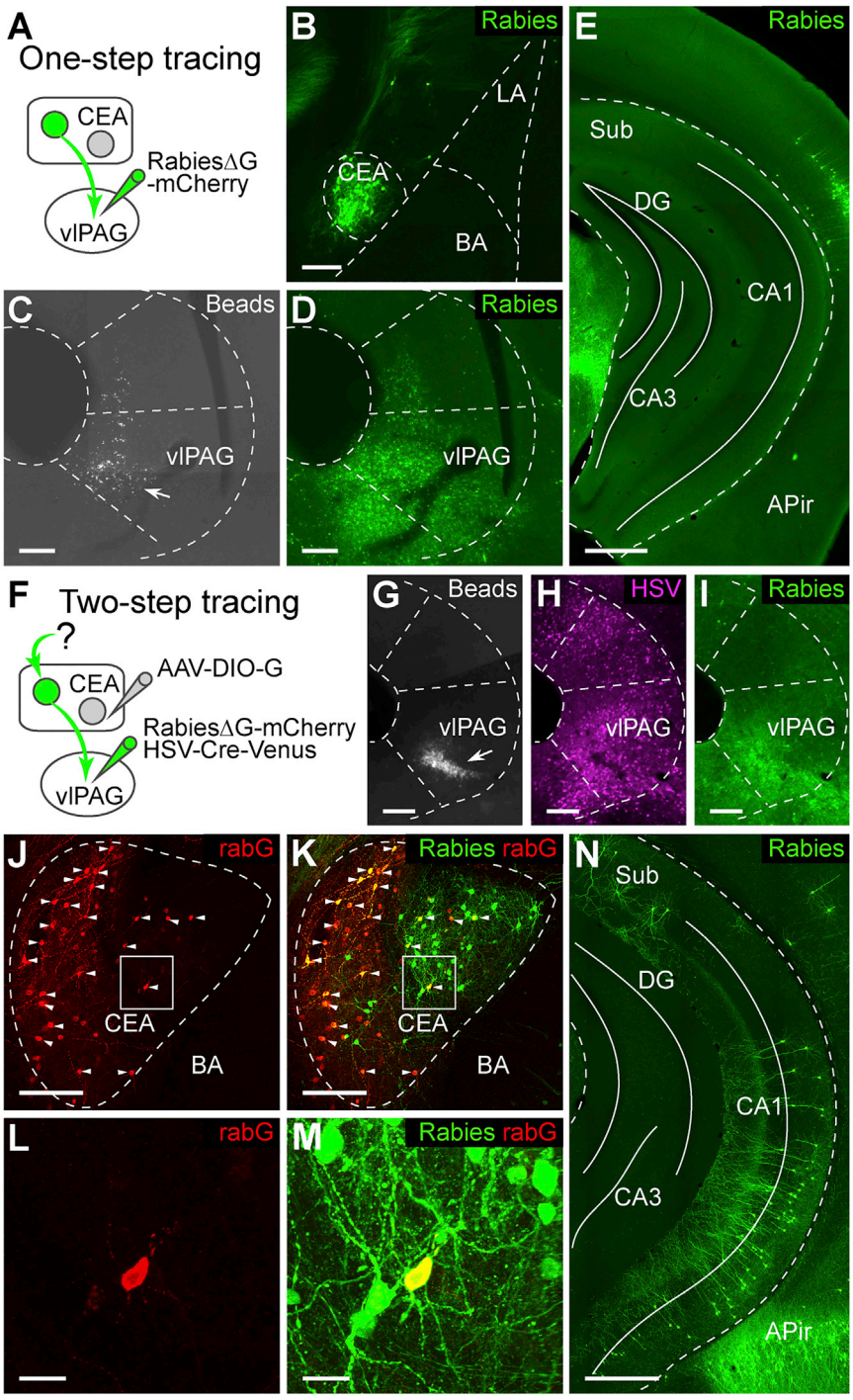

Figure 1. Hippocampal Projection onto vlPAG-Projecting CEA Output Neurons Identified by Rabies Virus-Mediated *trans*-synaptic Tracing

(A) Injection scheme illustrating experimental design for non-*trans*-synaptic retrograde tracing from the vlPAG to the CEA (one-step tracing from vlPAG). RabiesΔG-mCherry was injected locally into vlPAG.

(B) Example picture showing rabiesΔG-mCherry-labeled cells (green) in CEA after injections depicted in (A).

(C and D) Examples showing blue beads (C, arrow) and rabiesΔG-mCherry (D, green) co-injected into vlPAG.

(E) Example picture showing no cells were labeled by rabiesΔG-mCherry in vHC after injections depicted in (A).

(F) Injection scheme illustrating experimental design for *trans*-synaptic tracing from vlPAG-projecting CEA output neurons (two-step tracing from vlPAG). RabiesΔG-mCherry and HSV-Cre-Venus were co-injected into vlPAG. AAV-DIO-G was injected into the CEA.

(G–I) Examples showing blue beads (G, arrow), HSV-Cre-Venus (H, magenta), and rabiesΔG-mCherry (I, green) co-injected into vlPAG.

(J–M) Example pictures showing immunostaining for rabG (J, red) overlaid with staining for rabiesΔG-mCherry (K, green) in the CEA. Arrows indicate starter cells co-stained for rabiesΔG-mCherry and rabG. Magnifications of boxed areas in (J) and (K) are shown in (L) and (M), respectively.

(N) Example picture showing rabiesΔG-mCherry-labeled cells (green) in vHC after injections depicted in (F).

Scale bars, 500 μm (E and N) and 25 μm (L and M); all other panels, 200 μm. Abbreviations: Sub, subiculum; DG, dentate gyrus; APir, amygdalopiriform transition area, CA1: field CA1 of hippocampus; CA3, field CA3 of hippocampus. Blue beads are shown in gray, rabies-labeled in green, HSV-labeled in magenta, and rabG-stained cells in red.

See also Figure S1.

canine adenovirus type 2 expressing Cre-recombinase (CAV-Cre) (Soudais et al., 2001) into the CEA and AAV-DIO-ChR2 into the vHC and labeled vlPAG-projecting CEA neurons by injecting retrogradely transported fluorescent latex beads (retrobeads or RBs) into the vlPAG (Figures 3A and 3B). We then tested whether the CEA-projecting vHC neurons make functional connections onto CEA neurons by performing patch clamp recordings in acute brain slices (Figure 3C). Optogenetic stimulation of vHC afferents revealed functional glutamatergic excitatory inputs onto CEA neurons (Figures 3D and 3E). When recorded in on-cell configuration, light stimulation alone was able to elicit action potentials in 17 out of 43 cells (Figure 3D). In whole-cell configuration, excitatory post-synaptic currents (EPSCs) were evoked in 52 out of 64 CEA cells from 5 mice (81.3% connectivity; Figures 3E and 3F). Out of these, 28 were identified as vlPAG-projecting CEA neurons by RB labeling (23 with inputs, 82.1% connectivity; Figure S2A). Light-evoked EPSCs show average amplitudes of 195.3 ± 38.4 pA (n = 30; only RB+ cells: 186.7 ± 47.6 pA, n = 14; Figures 3G and S2B) and short latencies to EPSC peaks

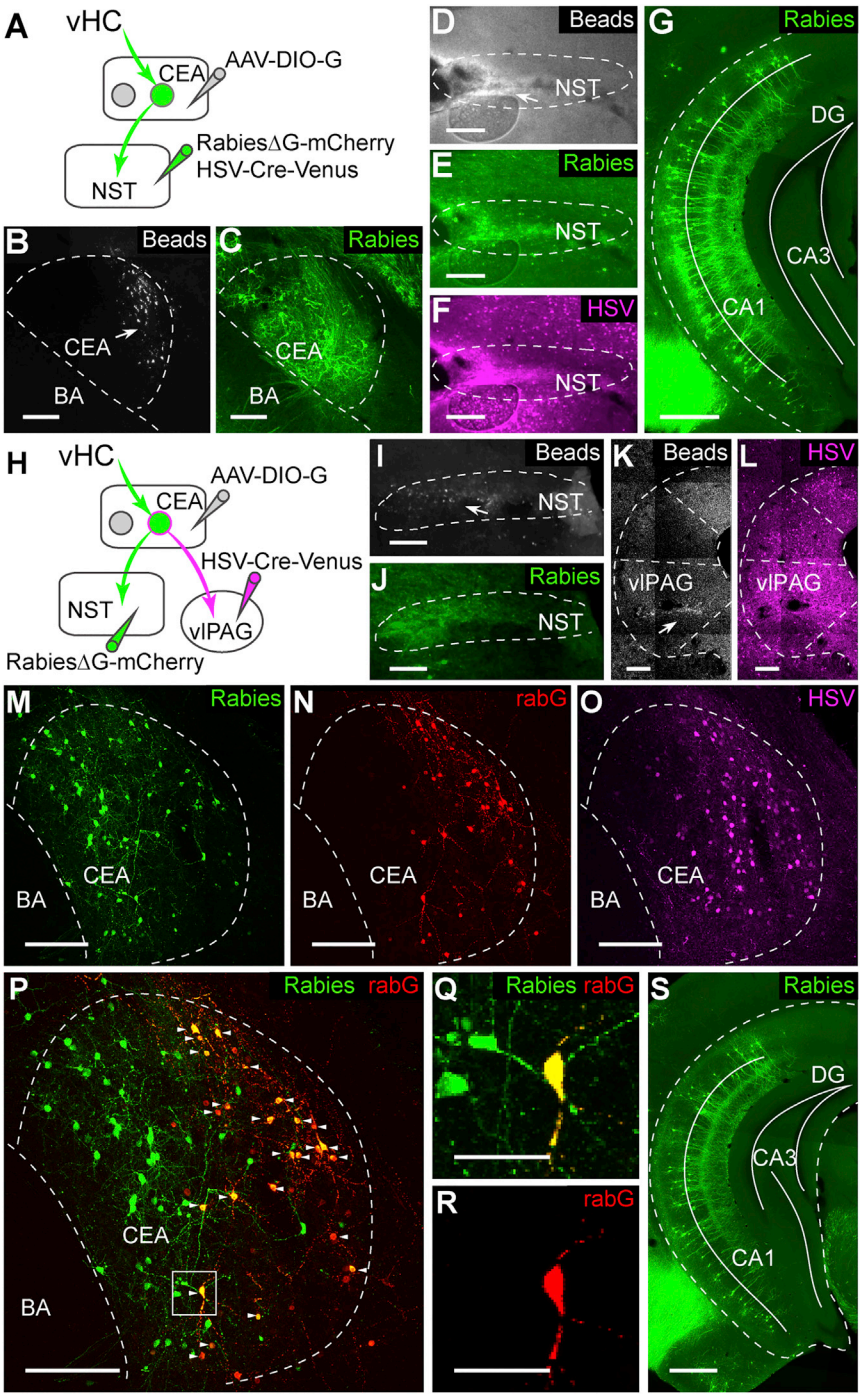

Figure 2. vHC Neurons Are Di-synaptically Connected to NST

(A) Scheme illustrating experimental design used for *trans*-synaptic retrograde tracing from the NST.

(B) Example picture showing injection site injected with a mixture of AAV-DIO-G and beads (arrow).

(C) Example picture showing rabies infection in the CEA.

(D–F) Example pictures showing infections by rabies (E, green), HSV-Cre-Venus (F, magenta), and co-injected beads (D) in the NST.

(G) Example picture showing rabies-labeled cells in vHC after injections depicted in (A).

(H) Scheme illustrating experimental strategy used for *trans*-synaptic tracing of presynaptic inputs to CEA neurons projecting to both the NST and the vlPAG.

(I and J) Example pictures showing co-injection of rabies (J) and beads (I, arrow) into the NST.

(K and L) Examples for HSV infection (L) and co-injected beads (K, arrow) in vlPAG.

(M–P) Example pictures showing rabies-labeled neurons (green, M), immunostaining for rabG (red, N), HSV-Cre-Venus-labeled neurons (magenta, O), and the overlay (P) in the CEA. Arrows point to starter cells co-stained for rabies and rabG.

(Q and R) Magnification of boxed area in (P) displaying an identified starter cell.

(S) Example picture showing rabies-labeled cells in vHC after injections depicted in (H).

Scale bars, 500 μm (G and S) and 50 μm (Q and R); all other panels, 200 μm.

See also Figure S1.

(all: 6.8 ± 0.3 ms; RB+ cells: 7.1 ± 0.6 ms; Figures 3H and S2C). Bath-application of the sodium channel blocker tetrodotoxin (TTX, 1 μM) did not completely abolish EPSC amplitudes (25.0% ± 3.9% of baseline, n = 5 cells; Figures 3I, S2D, and S2E), indicating that inputs were monosynaptic. EPSCs were completely blocked by the AMPA (α-Amino-3-hydroxy-5-methyl-4-isoxazolepropionic acid)-type glutamate receptor antagonist 6-cyano-7-nitroquinoxaline-2,3-dione (CNQX, 10 μM; Figures 3I and S2D). Finally, we measured the impact of vHC afferents on the input-output functions of CEA neurons in current-clamp configuration and found that stimulation of vHC afferents increased CEA neuron excitability (Figure 3J). Photostimulation of vHC afferents not only decreased the latency to the first spike elicited by current injections (baseline, 58 ± 23 ms; light, 30 ± 14 ms; n = 19 cells; Figures 3K and S2F), but also led to an excitatory shift in the input-output curves (baseline, I_{half} = 109.8 pA, light, I_{half} = 97.0 pA; n = 14 cells; Figures 3L and S2G). Together, and consistent with the anatomical and immunohistochemical experiments, these data demonstrate that vHC forms a glutamatergic, monosynaptic, and excitatory connection onto vlPAG-projecting CEA output neurons.

Separate vHC Neurons Project to CEA and BA

The vHC projection to the BA is believed to be important for transmitting contextual information to the amygdala (Maren et al., 2013). We thus examined whether the same vHC neurons would send divergent projections to both the BA and the CEA or

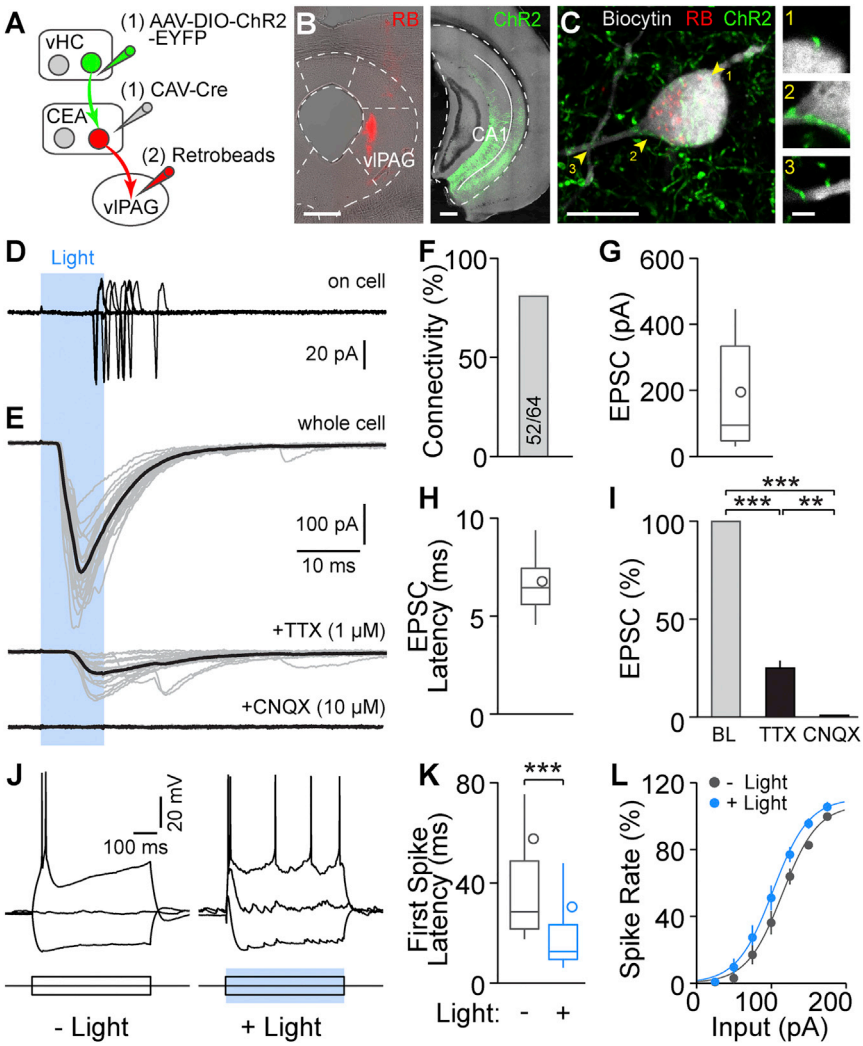

Figure 3. vHC Functionally Targets Output Neurons in the CEA

(A) Scheme illustrating sequential injections to express ChR2 in axons projecting from the vHC to the CEA and to label vlPAG-projecting output neurons in the CEA. CAV-Cre was injected into the CEA and AAV-DIO-ChR2-EYFP was injected into vHC. 4 weeks later, RBs were injected into the vlPAG.

(B) Left: RB injection into vlPAG; scale bar, 400 μm. Right: ChR2 expression in vHC; scale bar, 400 μm.

(C) Left: confocal image of an RB-labeled CEA output neuron filled with biocytin during recording; scale bar, 10 μm. Right: single planes of putative synaptic contacts between ChR2-expressing vHC afferents and the CEA neuron highlighted in the left image; scale bar, 2 μm.

(D) Example recording showing that vHC fiber photostimulation can elicit action potentials in a CEA output neuron (recorded in on-cell configuration; 17 out of 43 cells).

(E) Top: example recordings of blue light-evoked excitatory postsynaptic currents (EPSCs) in an RB-labeled neuron. Middle: light-evoked EPSCs from the same cell recorded in the presence of 1 μM TTX. Bottom: bath application of 10 μM CNQX completely abolishes light-evoked EPSCs. The average of the traces is shown in black.

(F) Connectivity from vHC afferents to CEA neurons was 81.3% (52 out of 64 cells from 5 mice).

(G and H) Summary of EPSC amplitudes and EPSC peak latencies in recorded CEA neurons. Data are presented as median with 25/75 percentile (box) and 10–90 percentile (whiskers); the circle indicates mean; n = 30 cells.

(I) EPSC amplitudes (normalized to baseline, BL) are reduced in the presence of TTX and completely abolished by application of CNQX; data are presented as mean ± SEM, n = 5 cells. Repeated measures (RM) one-way ANOVA revealed a significant difference between EPSC amplitudes in BL, TTX, and CNQX conditions ($F_{1.003,\ 4.012} = 511.3$, $p < 0.0001$). Tukey's multiple comparisons test revealed that EPSC amplitudes in BL, TTX, and CNQX conditions are all significantly different from each other.

(J) Excitability of CEA neurons with and without vHC afferent activation was assessed by depolarizing current steps. Left: example recording of baseline condition, −100 pA, 0 pA, and +100 pA steps are displayed. Right: example recording with the same current steps and paired blue-light stimulation. Note an action potential was evoked at a holding potential of −70 mV by vHC fiber photostimulation alone.

(K) Latency to the first action potential in response to somatic current injection of +100 pA is significantly shorter when paired with vHC fiber activation (Wilcoxon matched-pairs signed rank test, $p < 0.0001$). Data are presented as median with 25/75 percentile (box) and 10–90 percentile (whiskers); the circle indicates mean; n = 19 cells.

(L) vHC fiber photostimulation increases the excitability of CEA neurons. Spike rate is normalized to the maximum frequency in baseline condition of each cell. Sigmoidal curve fitting reveals a significant shift to the left of input-output curves with vHC fiber activation (−12.7 pA shift; I_{half} baseline 109.8 pA, I_{half} light 97.0 pA; paired t test, $p < 0.001$; n = 14 cells) without affecting rate or maximum output. Data are presented as mean ± SEM, n = 15 cells.

See also Figure S2.

whether these two pathways would involve distinct subpopulations of vHC neurons. To test these two possibilities, we used a dual-color retrograde tracing approach. In order to prevent contamination due to infection of en-passant vHC axons targeting the BA (Figures S3A and S3B), we took advantage of EnVA (glycoprotein from subgroup A avian sarcoma and leucosis virus) pseudotyped rabies to specifically identify CEA-projecting vHC neurons using *trans*-synaptic rabies tracing. Because the CEA almost exclusively contains GABAergic neurons (Ehrlich et al., 2009), we expressed the avian retroviral EnVA receptor (TVA) selectively in GABAergic cells by crossing a conditional TVA mouse line (Seidler et al., 2008) with a *GAD2*^{Cre} mouse line (glutamic acid decarboxylase 2) (Taniguchi et al., 2011). Subsequent co-injection of EnVA-pseudotyped rabiesΔG-mCherry (rabiesΔG-mCherry-EnVA) and AAV-DIO-G into the CEA revealed CEA-projecting vHC neurons. BA-projecting vHC neurons were labeled by direct retrograde tracing using HSV-GFP injected into the BA (Figures 4A–4E). Analysis showed that only 3% of

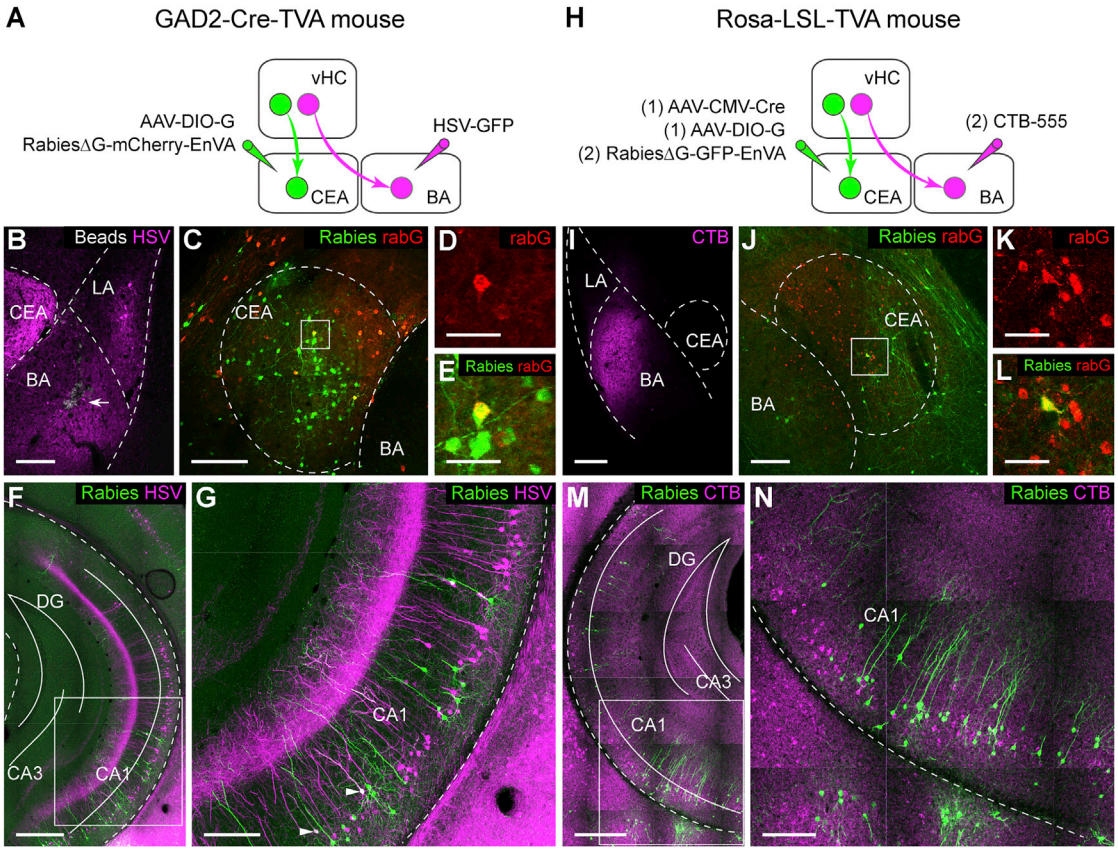

Figure 4. Distinct Groups of vHC Neurons Project to CEA and BA

(A) Scheme for dual retrograde tracings in GAD2-Cre-TVA mice. Simple retrograde tracing from the BA with HSV-GFP was combined with *trans*-synaptic tracing from local GABAergic cells in the CEA upon co-injection of rabiesΔG-mCherry-EnVA and AAV-DIO-G.

(B) Example picture showing co-injection of HSV-GFP (magenta) and beads (arrow) into the BA.

(C) Example showing rabiesΔG-mCherry-EnVA labeling (green) and immunostaining for rabG (red) in the CEA after injections depicted in (A).

(D and E) Magnification of the boxed area in (C) showing a starter cell positive for both rabG (D) and rabiesΔG-mCherry-EnVA (E), respectively.

(F and G) Example picture showing rabiesΔG-mCherry-EnVA- (green) and HSV-GFP- (magenta) labeled cells in vHC after injections depicted in (A). Magnification of the boxed area in (E) is shown in (G); two neurons (arrows) were co-labeled by rabiesΔG-mCherry-EnVA and HSV-GFP.

(H) Scheme for sequential injections in the CEA and the BA in Rosa-LSL-TVA mice. AAV-CMV-Cre and AAV-DIO-G were first injected into the CEA, enabling retrograde *trans*-synaptic tracing from all types of CEA neurons. 2 weeks later, rabiesΔG-GFP-EnVA was injected into the CEA and CTB-555 was injected into the BA.

(I) Example picture showing CTB-555 injection in the BA.

(J) Example showing rabiesΔG-GFP-EnVA labeling (green) and immunostaining for rabG (red) in the CEA after injections depicted in (H).

(K and L) Magnification of boxed area in (J), including an identified starter cell.

(M and N) Example showing rabies- (green) and CTB-555- (magenta) labeled cells in vHC after injections depicted in (H). Magnification of boxed area in (M) is shown in (N).

Scale bars, 50 μm (D, E, K and L) and 500 μm (G and N); all other panels, 200 μm. Blue beads are shown in gray, rabies-labeled cells in green, HSV-labeled cells in magenta, CTB and CTB-labeled cells in magenta, and rabG-stained cells in red.

See also Figure S3.

the rabiesΔG-mCherry-labeled cells were co-labeled with HSV-GFP (rabiesΔG-mCherry: 297 cells; HSV-GFP: 696 cells; co-labeled: 9 cells; n = 1 animal; Figures 4F and 4G). To avoid any potential bias caused by viral tropisms, we repeated the experiment using cholera toxin B-alexa 555 (CTB-555) instead of HSV-GFP and rabiesΔG-GFP-EnVA instead of rabiesΔG-mCherry-EnVA (Figures 4H–4L; see STAR Methods). Consistent with the first approach, we found that only 3.6% ± 2.5% of rabiesΔG-GFP-labeled cells were co-labeled with CTB-555 (rabiesΔG-GFP: 393 ± 108 cells; CTB-555: 1792 ± 867 cells; co-labeled: 11 ± 6 cells; n = 3 animals; Figures 4M and 4N). Moreover, a comparison of the 3D density distribution of vHC neurons projecting to the BA or the CEA revealed that CEA-projecting neurons are located more ventrally than BA-projecting neurons (Figure S3C). Finally, given that the BA sends a strong projection to the vHC (Pitkänen et al., 2000), we examined whether BA-projecting and CEA-projecting vHC neurons would receive input from the BA using a conditional rabies tracing approach. Interestingly, these experiments revealed that the BA strongly projects onto CEA-projecting vHC cells, but also

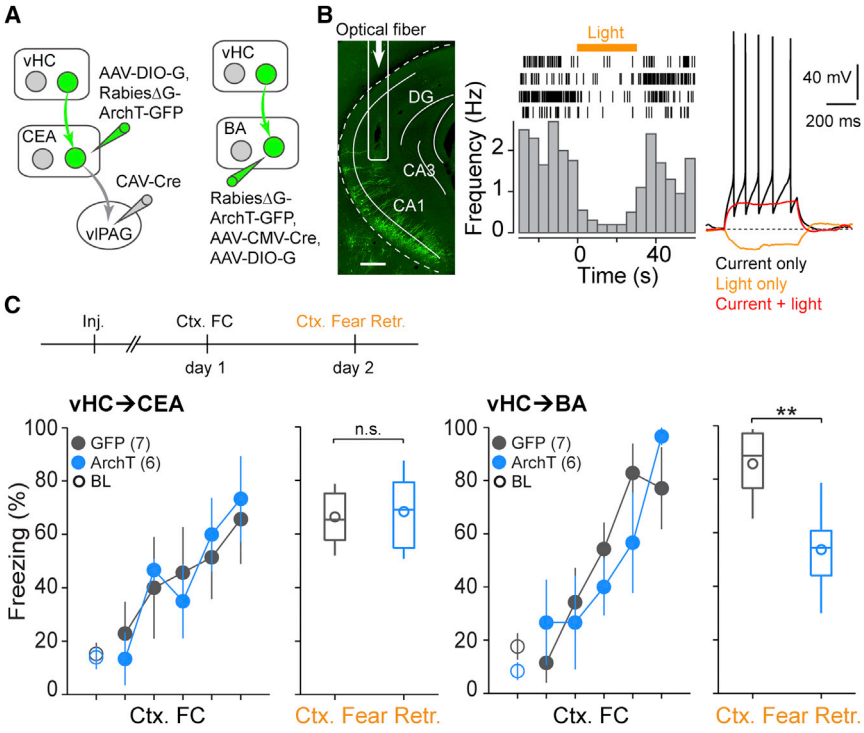

Figure 5. Distinct Roles for vHC→CEA and vHC→BA Pathways in Contextual Fear Memory Retrieval

(A) Scheme for labeling vHC neurons in vHC→CEA and vHC→BA pathways with rabiesΔG-ArchT-GFP.

(B) Left: CEA-projecting vHC neurons are labeled with rabiesΔG-ArchT-GFP after *trans*-synaptic tracing from vlPAG-projecting neurons in CEA as depicted in (A). Arrow: optical fiber location in vHC. Scale bar, 400 μm. Middle: raster plots (top) and peri-stimulus time histogram (bottom) illustrating yellow light-induced inhibition (yellow bar, 30 s) of single-unit activity in vHC after rabiesΔG-ArchT-GFP infection. Right: example recording from a vHC neuron infected by rabiesΔG-ArchT-GFP. Black, spikes evoked by a 60 pA current step; red, no spikes were evoked when the same current step was paired with yellow light stimulation; yellow, hyperpolarization elicited by yellow light stimulation; dashed gray line, the membrane potential at −60 mV.

(C) Top: scheme illustrating the behavioral paradigm used to test the functional role of vHC neurons in contextual fear retrieval. Yellow light was on during the entire contextual fear retrieval session (5 min). Bottom: summary data (mean ± SEM) of freezing during contextual fear conditioning (Ctx. FC, scatterplots) and subsequent contextual fear retrieval. Ctx. Fear Retr.: boxplots showing 25th, 50th, and 75th percentile (box and line), minimal and maximal values (whisker), and the mean value (circle) in animals with labeling for CEA- (left) and BA-projecting neurons (right). During Ctx. FC, the first data point represents the 2 min baseline (BL, open circles) and the rest represent the 10 s period before each US (reflecting inter-US freezing, filled circles). ArchT-mediated inhibition of the vHC→CEA pathway does not affect contextual fear retrieval (control, 66.4% ± 3.9%, n = 7; ArchT, 68.3% ± 6.2%, n = 6, Mann-Whitney U test, p = 0.8135). In contrast, inhibition of the vHC→BA pathway significantly impairs contextual fear retrieval (control, 85.7% ± 4.9%, n = 7; ArchT, 53.7% ± 6.7%, n = 6, Mann-Whitney U test, p = 0.007).

See also Figures S4, S5, and S6.

targets BA-projecting vHC cells (Figures S3D and S3E). Taken together, these data demonstrate that the vHC sends separate projections to the BA and the CEA by means of anatomically distinct subpopulations of vHC neurons, which, in turn, receive input from the BA.

Distinct Behavioral Roles for CEA and BA Pathways

Hippocampal input to the amygdala is believed to be required for context-dependent regulation of fear behavior, such as contextual fear or renewal of extinguished CS fear (Maren, 2001; Maren et al., 2013; Maren and Quirk, 2004). Accordingly, vHC is expected to show context-specific encoding during fear renewal. Indeed, using in vivo Ca^{2+} imaging of vHC neurons in freely moving mice, we found that vHC neurons exhibited context-specific activity patterns when mice entered the extinction or renewal contexts from the home cage with a subset of neurons biased toward the renewal context (Figure S4A–S4G). Given our finding that the vHC sends parallel and separate projections to distinct amygdala sub-nuclei, this raises the question whether these two pathways cooperate in regulating fear behavior in a context-dependent manner or whether they are involved in different aspects of contextually regulated fear.

To specifically investigate the behavioral role of vHC projections to the BA and the CEA, we generated a rabies strain expressing the inhibitory opsin ArchT (rabiesΔG-ArchT-GFP) (Han et al., 2011). To target the vHC→CEA pathway, we injected CAV-Cre into the vlPAG and AAV-DIO-G into the CEA, followed by an injection of rabiesΔG-ArchT-GFP into the CEA (Figure 5A). Because rabiesΔG-ArchT-GFP mainly infected local neurons around the injection site in the CEA and was only inefficiently taken up by vHC axon terminals (Figures S4H and S4I), this approach allowed us to specifically target vHC cells connecting to CEA output neurons that project to the vlPAG. To target the vHC→BA pathway, we injected a mixture of AAV-CMV-Cre and AAV-DIO-G and rabiesΔG-ArchT-GFP into the BA (Figure 5A; see STAR Methods). After the injections, we bilaterally implanted optical fibers into the vHC (Figures 5B and S5). Both in vivo single unit recordings and in vitro whole-cell patch clamp recordings confirmed that yellow light stimulation was able to inhibit the activity of rabiesΔG-ArchT-GFP-infected neurons (two light-inhibited units recorded from two mice and seven light-inhibited cells recorded in acute brain slices from two mice; Figures 5B and S4J).

We first tested the role of the vHC projections to the BA and the CEA in classical contextual fear conditioning. In contextual fear conditioning, mice are exposed to a context in which they experience repeated unsignaled foot-shocks. Upon re-exposure to the same context, they exhibit freezing behavior. Two groups of mice infected with either rabiesΔG-ArchT-GFP or rabiesΔG-GFP were subjected to contextual fear conditioning,

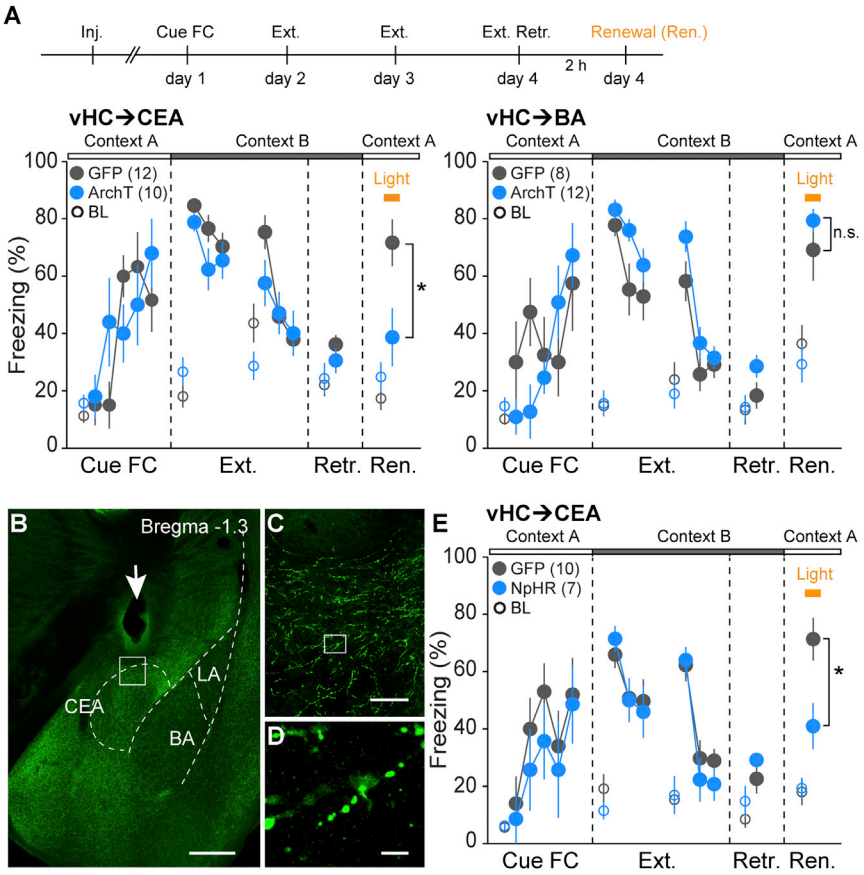

Figure 6. Distinct Roles for vHC→CEA and vHC→BA Pathways in Context-Dependent Fear Renewal

(A) Top: scheme illustrating the behavioral paradigm used to test the functional role of vHC neurons in fear renewal. On day 4, fear renewal (Ren.) was induced 2 hr after extinction memory retrieval test (Ext. Retr.). During the renewal session, the entire CS (tone) was paired with yellow-light stimulation (yellow bar) targeted to the vHC. Bottom: summary data (mean ± SEM) of CS-induced freezing in animals injected with rabiesΔG-ArchT-GFP (blue) compared to control mice injected with rabiesΔG-GFP (gray). Freezing during extinction and extinction retrieval sessions is shown in blocks of 4 CSs. Freezing in all other sessions is shown for single CSs. Open circles indicate 2 min baseline (BL) freezing for each behavioral session. Inhibition of the vHC→CEA pathway, but not the vHC→BA pathway, significantly reduces freezing during fear renewal (vHC→CEA: control, 71.7% ± 8.1%, n = 12; ArchT, 38.7% ± 10.1%, n = 10, Mann-Whitney U test, p = 0.0294; vHC→BA: control, 69.2% ± 10.8%, n = 8; ArchT, 78.9% ± 3.7%, n = 12, Mann-Whitney U test, p = 0.6832).

(B) eNpHR3.0-mediated inhibition of vHC axon terminals in the CEA. eNpHR3.0 expression in CEA-projecting axons was achieved by injection of CAV-Cre into the CEA and injection of AAV-DIO-eNpHR3.0-EYFP into the vHC. Arrow: optic fiber location above the CEA. Scale bar, 0.5 mm.

(C) Magnification of boxed area in (B). Scale bar, 50 μm.

(D) Magnification of boxed area in (C). Scale bar, 5 μm.

(E) Summary data (mean ± SEM) of CS-induced freezing in animals injected with AAV-DIO-eNpHR3.0 (blue, NpHR group) compared to control mice injected with AAV-DIO-GFP (gray, control group). Freezing during extinction and extinction retrieval sessions is shown in blocks of 4 CSs. Freezing in all other sessions is shown for single CSs. Open circles indicate 2 min baseline (BL) freezing for each behavioral session. Inhibition of the vHC→CEA axons in the CEA significantly reduces freezing during fear renewal (control, 71.3% ± 7.4%, n = 10; NpHR, 41.0% ± 8.0%, n = 7, Mann-Whitney U test, p = 0.0102).

See also Figures S4, S5, and S6.

and memory retrieval was tested 24 hr later with light stimulation. Whereas inhibition of the vHC→BA projection resulted in a significant reduction in context-induced freezing behavior, inhibiting the vHC→CEA projection had no effect (BA: control, 85.7% ± 4.9% of time spent freezing, n = 7 mice; ArchT, 53.7% ± 6.7%, n = 6; p = 0.007, Mann-Whitney U test; CEA: control, 66.4% ± 3.9%, n = 7; ArchT, 68.3% ± 6.2%, n = 6; p = 0.8135, Mann-Whitney U test; Figure 5C).

Given the role of the vHC and the amygdala in the contextual gating of cued fear memory retrieval (Herry et al., 2008; Hobin et al., 2003; Orsini et al., 2011), we next examined the role of the vHC projections to the BA or the CEA in fear renewal. Again, we compared two groups of animals injected with either rabiesΔG-ArchT-GFP or rabiesΔG-GFP. Both groups were subjected to cued fear conditioning and 2 days of subsequent extinction training in a different context (Figure 6A). On day 4, both groups exhibited low freezing levels to the CS in the extinction context, indicating the formation of a long-term extinction memory (Figure 6A). We then tested fear renewal by exposing mice to the CS in the original fear conditioning context. Notably, fear renewal was almost completely abolished in animals in which the vHC→CEA pathway was inhibited during CS presentation (control, 71.7% ± 8.1%, n = 12; ArchT, 38.7% ± 10.1%, n = 10; Mann-Whitney U test, p = 0.029), without any effect on CS fear retrieval prior to extinction training (control: 62.2% ± 5.1%, n = 6; ArchT: 58.9% ± 3.2%, n = 6; Mann-Whitney U test, p = 0.426; Figure S4K). In contrast, animals with inhibition of the vHC→BA pathway exhibited normal fear renewal (control, 69.2% ± 10.8%, n = 8; ArchT, 78.9% ± 3.7%, n = 12; Mann-Whitney U test, p = 0.68). To address the possibility that the behavioral effects were caused by inhibition of collateral projections to other brain regions, we performed optogenetic manipulations of vHC→CEA axonal terminals. We injected CAV-Cre into the CEA and AAV-DIO-eNpHR3.0-EYFP (Gradinaru et al., 2010) into the vHC and implanted optical fibers above the CEA (Figures 6B–6D, S5, and S6B). Indeed, inhibition of the vHC→CEA axonal terminals in the CEA significantly reduced freezing during fear renewal (control, 71.3% ± 7.4%, n = 10; NpHR [Halorhodopsin], 41.0% ± 8.0%, n = 7, Mann-Whitney U test, p = 0.0102, Figure 6E). Taken together, these results demonstrated a double dissociation of the roles of the vHC→BA and vHC→CEA pathways in contextual regulation of fear behavior.

DISCUSSION

Both the dorsal and ventral hippocampus have been shown to be important for context-dependent fear responses (Kim and Fanselow, 1992; Maren, 2001; Maren and Quirk, 2004; Phillips and LeDoux, 1992), but only the vHC directly projects to amygdala (Pitkänen et al., 2000). In this study, using a combination of *trans*-synaptic circuit tracing together with physiological and optogenetic approaches, we have identified two parallel vHC→amygdala pathways that mediate fundamentally distinct roles of context in associative learning. Whereas the vHC projection to the BA is required for the retrieval and/or expression of fear behavior conditioned to the context itself, the projection to the CEA is not necessary. In contrast, even though the direct projection from the vHC onto midbrain-targeting CEA neurons is not required for contextual freezing per se, it mediates contextual gating of cued fear memory retrieval.

Our finding that the vHC→BA pathway is necessary for the retrieval and/or expression of conditioned freezing behavior elicited by the context in itself is consistent with previous experiments demonstrating impaired contextual freezing upon lesion or pharmacological inactivation of the vHC or the BA (Maren and Holt, 2004; Richmond et al., 1999). In the BA, the vHC afferents contact both excitatory principal neurons (PNs) and local GABAergic interneurons (Bazelot et al., 2015; Hübner et al., 2014). Moreover, given that the BA contains functionally and anatomically distinct subpopulations of PNs with opposite roles in fear behavior (Herry et al., 2008; Senn et al., 2014), it is possible that the behavioral relevance of vHC inputs to the BA is not limited to the retrieval and/or expression of contextual fear, but might also be involved in the acquisition or extinction of contextual fear and appetitive behaviors (Goshen et al., 2011; Maren, 1999; Maren and Fanselow, 1995; Maren and Holt, 2004; Tracy et al., 2001).

Dual tracing experiments revealed that vHC neurons projecting to the BA or the CEA are anatomically distinct neuronal subpopulations. Even though the spread along the ventral-dorsal axis was slightly different for BA- and CEA-projecting neurons, they were mostly intermingled in a salt-and-pepper-like manner. Such a circuit organization might facilitate local interactions between different vHC output pathways involved in the contextual regulation of distinct behaviors (Ciocchi et al., 2015) and has also been described in other brain areas, including the cortex (Hattox and Nelson, 2007), the striatum (Surmeier et al., 2007), and the amygdala (Senn et al., 2014).

The finding that the vHC→BA pathway is not required for the contextual gating of cued fear memory retrieval is surprising in light of previous studies. In fact, lesion or pharmacological inactivation of the vHC or the BA interferes with fear renewal (Herry et al., 2008; Hobin et al., 2006), and so does anatomical disconnection of the two structures (Orsini et al., 2011). Moreover, electrical stimulation of vHC axons activates BA fear neurons (Herry et al., 2008). Given that functional inactivation of the vHC→BA pathway interfered with the expression of contextual fear and that the two structures are reciprocally connected, the results of the present study are unlikely to reflect a technical failure to silence BA-projecting vHC neurons, but rather suggests that fear renewal deficits in lesion studies were caused by the interruption of information flow from the BA to the vHC rather than the opposite direction. Consistent with this notion, we found that BA cells projecting to the vHC target CEA-projecting vHC neurons. Our findings are thus consistent with a model in which vHC integrates information from the BA and possibly the dorsal HC and broadcasts this information to various downstream targets, such as the CEA or the mPFC (Cenquizca and Swanson, 2007; Hoover and Vertes, 2007), two structures sending converging projections to midbrain circuits controlling defensive behavior (Ciocchi et al., 2010; Courtin et al., 2014). Thus, contextualization of conditioned fear responses may involve a multisite integration process including the mPFC, CEA, and PAG.

Notably, we found that CEA-projecting vHC neurons synapse onto CEA output neurons projecting to downstream targets in the mid- and hindbrain, such as the vlPAG or NST. Even though CEA output neurons are located both in the CEm and the CEl (Ciocchi et al., 2010; Penzo et al., 2014), most of the vHC axonal afferents are found in the CEm (Figure S4L) (Cenquizca and Swanson, 2007; Kishi et al., 2006). Because vlPAG-projecting CEA neurons receive inputs from the BLA, it is conceivable that contextual gating of cued fear responses is mediated by functional interactions of converging BLA and vHC afferents at the level of individual CEA output neurons or at the local circuit level.

Our results indicate that CEA output neurons receiving vHC input project, at least in part, to both the vlPAG and the NST. This does not exclude the possibility that some CEA output neurons are target-specific (Viviani et al., 2011), but it is consistent with single-cell axonal tracings demonstrating that CEA output neurons exhibit multiple axonal collaterals in vlPAG, NST, and other brainstem nuclei (Veinante and Freund-Mercier, 2003). Taken together, our findings indicate that, by means of a direct input onto CEA output neurons, the vHC can route contextual information into a pathway directly controlling multiple aspects of a fear response, including motor, autonomic, and possibly neuroendocrine components.

Behavioral studies indicate that context can have fundamentally different roles during associative learning (Bouton, 2002, 2004; Urcelay and Miller, 2010). Context can act as a complex cue consisting of a combination of external and internal sensory inputs, which becomes associated with positive or negative outcomes, such as during contextual fear conditioning. Context can also have a modulatory role and gate the retrieval or expression of cue-outcome associations, as seen upon renewal of previously extinguished fear responses (Bouton, 2002; Bouton et al., 2006). Recent evidence from behavioral studies indicates that the relative roles of these two functions of context interact, but that they can be dissociated depending on a number of parameters, including inter-trial intervals or CS-US contiguity (Urcelay and Miller, 2010, 2014). This raises the question of how behavioral dissociation relates to the organization of the underlying neuronal circuitry. Our findings thus demonstrate that context is processed in parallel hippocampal modules promoting distinct functions of context in associative learning, thereby allowing for robust associations of context with aversive outcomes

while preserving appropriate context-dependent behavioral flexibility.

STAR★METHODS

Detailed methods are provided in the online version of this paper and include the following:

- KEY RESOURCES TABLE
- CONTACT FOR REAGENT AND RESOURCE SHARING
- EXPERIMENTAL MODEL AND SUBJECT DETAILS
  - Animals
  - Cell Culture
- METHOD DETAILS
  - Virus preparations
  - Stereotaxic injections
  - Immunohistochemistry
  - Optogenetics and behavior
  - Slice electrophysiology
  - Immunohistochemistry
  - Optrode recordings of neurons infected with rabiesΔG-ArchT-GFP
  - 3D Reconstructions and quantitative analysis of anatomical tracings
  - Microendoscope imaging
- QUANTIFICATION AND STATISTICAL ANALYSIS

SUPPLEMENTAL INFORMATION

Supplemental Information includes six figures and can be found with this article online at http://dx.doi.org/10.1016/j.cell.2016.09.051.

AUTHOR CONTRIBUTIONS

C.X. initiated the project and performed most experiments and data analysis. P.B. and S.K. performed and analyzed in vitro slice experiments. J.P.F. performed and analyzed in vivo recordings. F.O. and E.M.C. generated the rabies variants, including rabiesΔG-ArchT-GFP. D.S. generated the ROSA-LSL-TVA mouse line. J.G., B.F.G., and M.J.S. established vHC imaging methods. J.G. designed, performed, and analyzed the in vivo imaging experiments. C.X. and A.L. conceived the project. C.X. and A.L. wrote the manuscript. All authors contributed to the experimental design and interpretation and commented on the manuscript.

ACKNOWLEDGMENTS

We thank all members of the A.L. lab and C. Herry for discussions and critical comments on the manuscript. We thank B. Roska and K. Balint for help with rabies virus production. We thank J. Luedke, C. Mueller, T.J. Lu, K. Bylund, A. Kovacevic, P. Argast, P. Buchmann, the FMI core facilities, and IT for technical assistance and analysis. We also thank K. Yonehara, P. Scheiffele, L. Xiao, T.G. Oertner, J.A.T. Young, K. Deisseroth, E. Boyden, E. Kremer, J.Z. Huang, S.H. Hughes, C.L. Cepko, M. Stadler, and S. Pettersson for sharing materials, mouse lines, and analysis tools. This work was supported by the Novartis Research Foundation, an ERC Advanced Grant (to A.L.), the National Center of Competences in Research: "SYNAPSY - The Synaptic Bases of Mental Diseases" (financed by the Swiss National Science Foundation) (to A.L.), an SNSF core grant (to A.L.), grants from the NIH (MH063912 and EY022577 to E.M.C.), the NIMH (to M.J.S.), EMBO Long-Term Fellowships (to X.C., J.P.F., and J.G.), NARSAD Young Investigator Awards (to J.P.F. and S.K.), and an SNSF Ambizione Fellowship (to J.G.). M.J.S. is a co-founder of and consults for Inscopix Inc., which makes the nVista microscope used here for imaging in freely behaving mice.

Received: January 8, 2016
Revised: June 29, 2016
Accepted: September 17, 2016
Published: October 20, 2016

REFERENCES

Bazelot, M., Bocchio, M., Kasugai, Y., Fischer, D., Dodson, P.D., Ferraguti, F., and Capogna, M. (2015). Hippocampal Theta Input to the Amygdala Shapes Feedforward Inhibition to Gate Heterosynaptic Plasticity. Neuron *87*, 1290–1303.

Bouton, M.E. (2002). Context, ambiguity, and unlearning: sources of relapse after behavioral extinction. Biol. Psychiatry *52*, 976–986.

Bouton, M.E. (2004). Context and behavioral processes in extinction. Learn. Mem. *11*, 485–494.

Bouton, M.E., and Swartzentruber, D. (1986). Analysis of the Associative and Occasion-Setting Properties of Contexts Participating in a Pavlovian Discrimination. J. Exp. Psychol. Anim. Behav. Process. *12*, 333–350.

Bouton, M.E., Westbrook, R.F., Corcoran, K.A., and Maren, S. (2006). Contextual and temporal modulation of extinction: behavioral and biological mechanisms. Biol. Psychiatry *60*, 352–360.

Cenquizca, L.A., and Swanson, L.W. (2007). Spatial organization of direct hippocampal field CA1 axonal projections to the rest of the cerebral cortex. Brain Res. Brain Res. Rev. *56*, 1–26.

Ciocchi, S., Herry, C., Grenier, F., Wolff, S.B., Letzkus, J.J., Vlachos, I., Ehrlich, I., Sprengel, R., Deisseroth, K., Stadler, M.B., et al. (2010). Encoding of conditioned fear in central amygdala inhibitory circuits. Nature *468*, 277–282.

Ciocchi, S., Passecker, J., Malagon-Vina, H., Mikus, N., and Klausberger, T. (2015). Brain computation. Selective information routing by ventral hippocampal CA1 projection neurons. Science *348*, 560–563.

Courtin, J., Chaudun, F., Rozeske, R.R., Karalis, N., Gonzalez-Campo, C., Wurtz, H., Abdi, A., Baufreton, J., Bienvenu, T.C., and Herry, C. (2014). Prefrontal parvalbumin interneurons shape neuronal activity to drive fear expression. Nature *505*, 92–96.

Dampney, R.A. (1994). Functional organization of central pathways regulating the cardiovascular system. Physiol. Rev. *74*, 323–364.

Davis, M. (1992). The role of the amygdala in fear and anxiety. Annu. Rev. Neurosci. *15*, 353–375.

Davis, M. (2000). The role of the amygdala in conditioned and unconditioned fear and anxiety. In The amygdala, J.P. Aggleton, ed. (Oxford, UK: Oxford University Press), pp. 213–288.

Ehrlich, I., Humeau, Y., Grenier, F., Ciocchi, S., Herry, C., and Lüthi, A. (2009). Amygdala inhibitory circuits and the control of fear memory. Neuron *62*, 757–771.

Fanselow, M.S., and Poulos, A.M. (2005). The neuroscience of mammalian associative learning. Annu. Rev. Psychol. *56*, 207–234.

Goshen, I., Brodsky, M., Prakash, R., Wallace, J., Gradinaru, V., Ramakrishnan, C., and Deisseroth, K. (2011). Dynamics of retrieval strategies for remote memories. Cell *147*, 678–689.

Gradinaru, V., Zhang, F., Ramakrishnan, C., Mattis, J., Prakash, R., Diester, I., Goshen, I., Thompson, K.R., and Deisseroth, K. (2010). Molecular and cellular approaches for diversifying and extending optogenetics. Cell *141*, 154–165.

Gross, C.T., and Canteras, N.S. (2012). The many paths to fear. Nat. Rev. Neurosci. *13*, 651–658.

Han, X., Chow, B.Y., Zhou, H., Klapoetke, N.C., Chuong, A., Rajimehr, R., Yang, A., Baratta, M.V., Winkle, J., Desimone, R., and Boyden, E.S. (2011). A high-light sensitivity optical neural silencer: development and application to optogenetic control of non-human primate cortex. Front. Syst. Neurosci. *5*, 18.

Hattox, A.M., and Nelson, S.B. (2007). Layer V neurons in mouse cortex projecting to different targets have distinct physiological properties. J. Neurophysiol. *98*, 3330–3340.

Herry, C., Ciocchi, S., Senn, V., Demmou, L., Müller, C., and Lüthi, A. (2008). Switching on and off fear by distinct neuronal circuits. Nature *454*, 600–606.

Hobin, J.A., Goosens, K.A., and Maren, S. (2003). Context-dependent neuronal activity in the lateral amygdala represents fear memories after extinction. J. Neurosci. *23*, 8410–8416.

Hobin, J.A., Ji, J., and Maren, S. (2006). Ventral hippocampal muscimol disrupts context-specific fear memory retrieval after extinction in rats. Hippocampus *16*, 174–182.

Hoover, W.B., and Vertes, R.P. (2007). Anatomical analysis of afferent projections to the medial prefrontal cortex in the rat. Brain Struct. Funct. *212*, 149–179.

Hübner, C., Bosch, D., Gall, A., Lüthi, A., and Ehrlich, I. (2014). Ex vivo dissection of optogenetically activated mPFC and hippocampal inputs to neurons in the basolateral amygdala: implications for fear and emotional memory. Front. Behav. Neurosci. *8*, 64.

Ji, J., and Maren, S. (2007). Hippocampal involvement in contextual modulation of fear extinction. Hippocampus *17*, 749–758.

Kapp, B.S., Frysinger, R.C., Gallagher, M., and Haselton, J.R. (1979). Amygdala central nucleus lesions: effect on heart rate conditioning in the rabbit. Physiol. Behav. *23*, 1109–1117.

Kim, J.J., and Fanselow, M.S. (1992). Modality-specific retrograde amnesia of fear. Science *256*, 675–677.

Kishi, T., Tsumori, T., Yokota, S., and Yasui, Y. (2006). Topographical projection from the hippocampal formation to the amygdala: a combined anterograde and retrograde tracing study in the rat. J. Comp. Neurol. *496*, 349–368.

Krettek, J.E., and Price, J.L. (1978). A description of the amygdaloid complex in the rat and cat with observations on intra-amygdaloid axonal connections. J. Comp. Neurol. *178*, 255–280.

LeDoux, J.E. (2000). Emotion circuits in the brain. Annu. Rev. Neurosci. *23*, 155–184.

LeDoux, J.E., Iwata, J., Cicchetti, P., and Reis, D.J. (1988). Different projections of the central amygdaloid nucleus mediate autonomic and behavioral correlates of conditioned fear. J. Neurosci. *8*, 2517–2529.

Lee, S.H., Marchionni, I., Bezaire, M., Varga, C., Danielson, N., Lovett-Barron, M., Losonczy, A., and Soltesz, I. (2014). Parvalbumin-positive basket cells differentiate among hippocampal pyramidal cells. Neuron *82*, 1129–1144.

Maren, S. (1999). Neurotoxic or electrolytic lesions of the ventral subiculum produce deficits in the acquisition and expression of Pavlovian fear conditioning in rats. Behav. Neurosci. *113*, 283–290.

Maren, S. (2001). Neurobiology of Pavlovian fear conditioning. Annu. Rev. Neurosci. *24*, 897–931.

Maren, S., and Fanselow, M.S. (1995). Synaptic plasticity in the basolateral amygdala induced by hippocampal formation stimulation in vivo. J. Neurosci. *15*, 7548–7564.

Maren, S., and Holt, W.G. (2004). Hippocampus and Pavlovian fear conditioning in rats: muscimol infusions into the ventral, but not dorsal, hippocampus impair the acquisition of conditional freezing to an auditory conditional stimulus. Behav. Neurosci. *118*, 97–110.

Maren, S., and Quirk, G.J. (2004). Neuronal signalling of fear memory. Nat. Rev. Neurosci. *5*, 844–852.

Maren, S., Phan, K.L., and Liberzon, I. (2013). The contextual brain: implications for fear conditioning, extinction and psychopathology. Nat. Rev. Neurosci. *14*, 417–428.

Mukamel, E.A., Nimmerjahn, A., and Schnitzer, M.J. (2009). Automated analysis of cellular signals from large-scale calcium imaging data. Neuron *63*, 747–760.

Orsini, C.A., Kim, J.H., Knapska, E., and Maren, S. (2011). Hippocampal and prefrontal projections to the basal amygdala mediate contextual regulation of fear after extinction. J. Neurosci. *31*, 17269–17277.

Osakada, F., and Callaway, E.M. (2013). Design and generation of recombinant rabies virus vectors. Nat. Protoc. *8*, 1583–1601.

Paxinos, G., and Franklin, K.B.J. (2001). The mouse brain in stereotaxic coordinates, Second Edition (San Diego: Academic Press).

Penzo, M.A., Robert, V., and Li, B. (2014). Fear conditioning potentiates synaptic transmission onto long-range projection neurons in the lateral subdivision of central amygdala. J. Neurosci. *34*, 2432–2437.

Petrovich, G.D., Canteras, N.S., and Swanson, L.W. (2001). Combinatorial amygdalar inputs to hippocampal domains and hypothalamic behavior systems. Brain Res. Brain Res. Rev. *38*, 247–289.

Phillips, R.G., and LeDoux, J.E. (1992). Differential contribution of amygdala and hippocampus to cued and contextual fear conditioning. Behav. Neurosci. *106*, 274–285.

Pitkänen, A., Savander, V., and LeDoux, J.E. (1997). Organization of intra-amygdaloid circuitries in the rat: an emerging framework for understanding functions of the amygdala. Trends Neurosci. *20*, 517–523.

Pitkänen, A., Pikkarainen, M., Nurminen, N., and Ylinen, A. (2000). Reciprocal connections between the amygdala and the hippocampal formation, perirhinal cortex, and postrhinal cortex in rat. A review. Ann. N Y Acad. Sci. *911*, 369–391.

Richmond, M.A., Yee, B.K., Pouzet, B., Veenman, L., Rawlins, J.N., Feldon, J., and Bannerman, D.M. (1999). Dissociating context and space within the hippocampus: effects of complete, dorsal, and ventral excitotoxic hippocampal lesions on conditioned freezing and spatial learning. Behav. Neurosci. *113*, 1189–1203.

Seidler, B., Schmidt, A., Mayr, U., Nakhai, H., Schmid, R.M., Schneider, G., and Saur, D. (2008). A Cre-loxP-based mouse model for conditional somatic gene expression and knockdown in vivo by using avian retroviral vectors. Proc. Natl. Acad. Sci. USA *105*, 10137–10142.

Sena-Esteves, M., Tebbets, J.C., Steffens, S., Crombleholme, T., and Flake, A.W. (2004). Optimized large-scale production of high titer lentivirus vector pseudotypes. J. Virol. Methods *122*, 131–139.

Senn, V., Wolff, S.B., Herry, C., Grenier, F., Ehrlich, I., Gründemann, J., Fadok, J.P., Müller, C., Letzkus, J.J., and Lüthi, A. (2014). Long-range connectivity defines behavioral specificity of amygdala neurons. Neuron *81*, 428–437.

Soudais, C., Laplace-Builhe, C., Kissa, K., and Kremer, E.J. (2001). Preferential transduction of neurons by canine adenovirus vectors and their efficient retrograde transport in vivo. FASEB J. *15*, 2283–2285.

Surmeier, D.J., Ding, J., Day, M., Wang, Z., and Shen, W. (2007). D1 and D2 dopamine-receptor modulation of striatal glutamatergic signaling in striatal medium spiny neurons. Trends Neurosci. *30*, 228–235.

Swanson, L.W., and Petrovich, G.D. (1998). What is the amygdala? Trends Neurosci. *21*, 323–331.

Tallone, T., Malin, S., Samuelsson, A., Wilbertz, J., Miyahara, M., Okamoto, K., Poellinger, L., Philipson, L., and Pettersson, S. (2001). A mouse model for adenovirus gene delivery. Proc. Natl. Acad. Sci. USA *98*, 7910–7915.

Taniguchi, H., He, M., Wu, P., Kim, S., Paik, R., Sugino, K., Kvitsiani, D., Fu, Y., Lu, J., Lin, Y., et al. (2011). A resource of Cre driver lines for genetic targeting of GABAergic neurons in cerebral cortex. Neuron *71*, 995–1013.

Thévenaz, P., Ruttimann, U.E., and Unser, M. (1998). A pyramid approach to subpixel registration based on intensity. IEEE Trans. Image Process. *7*, 27–41.

Tovote, P., Fadok, J.P., and Lüthi, A. (2015). Neuronal circuits for fear and anxiety. Nat. Rev. Neurosci. *16*, 317–331.

Tracy, A.L., Jarrard, L.E., and Davidson, T.L. (2001). The hippocampus and motivation revisited: appetite and activity. Behav. Brain Res. *127*, 13–23.

Urcelay, G.P., and Miller, R.R. (2010). Two roles of the context in Pavlovian fear conditioning. J. Exp. Psychol. Anim. Behav. Process. *36*, 268–280.

Urcelay, G.P., and Miller, R.R. (2014). The functions of contexts in associative learning. Behav. Processes *104*, 2–12.

Veening, J.G., Swanson, L.W., and Sawchenko, P.E. (1984). The organization of projections from the central nucleus of the amygdala to brainstem sites

involved in central autonomic regulation: a combined retrograde transport-immunohistochemical study. Brain Res. *303*, 337–357.

Veinante, P., and Freund-Mercier, M.J. (2003). Branching patterns of central amygdaloid nucleus efferents in the rat: single-axon reconstructions. Ann N Y Acad Sci *985*, 552–553.

Viviani, D., Charlet, A., van den Burg, E., Robinet, C., Hurni, N., Abatis, M., Magara, F., and Stoop, R. (2011). Oxytocin selectively gates fear responses through distinct outputs from the central amygdala. Science *333*, 104–107.

Wickersham, I.R., Lyon, D.C., Barnard, R.J., Mori, T., Finke, S., Conzelmann, K.K., Young, J.A., and Callaway, E.M. (2007). Monosynaptic restriction of transsynaptic tracing from single, genetically targeted neurons. Neuron *53*, 639–647.

Wolff, S.B., Gründemann, J., Tovote, P., Krabbe, S., Jacobson, G.A., Müller, C., Herry, C., Ehrlich, I., Friedrich, R.W., Letzkus, J.J., and Lüthi, A. (2014). Amygdala interneuron subtypes control fear learning through disinhibition. Nature *509*, 453–458.

Yonehara, K., Farrow, K., Ghanem, A., Hillier, D., Balint, K., Teixeira, M., Jüttner, J., Noda, M., Neve, R.L., Conzelmann, K.K., and Roska, B. (2013). The first stage of cardinal direction selectivity is localized to the dendrites of retinal ganglion cells. Neuron *79*, 1078–1085.

STAR★METHODS

KEY RESOURCES TABLE

REAGENT or RESOURCE	SOURCE	IDENTIFIER
Antibodies		
Guinea pig polyclonal anti-rabies glycoprotein (rabG)	Eurogentec, Belgium	N/A
Goat polyclonal anti-GFP	Abcam	Cat#AB6673; RRID: AB_305643
Rabbit polyclonal anti-mCherry	Abcam	Cat#AB28664; RRID: AB_777698
Mouse monoclonal anti-NeuN	Millipore	Cat#MAB377; RRID: AB_2298772
Rabbit polyclonal anti-GABA	Sigma	Cat#A2052; RRID: AB_477652
Rabbit polyclonal anti-CaMKII	Abcam	Cat#AB52476; RRID: AB_868641
Rabbit polyclonal anti-GFP	Invitrogen	Cat#A11122; RRID: AB_2307355
Goat polyclonal anti-guinea pig alexa 647	Invitrogen	Cat#A21450; RRID: AB_141882
Donkey polyclonal anti-goat alexa 488	Invitrogen	Cat#A11055; RRID: AB_142672
Donkey polyclonal anti-rabbit alexa 488	Invitrogen	Cat#A21206; RRID: AB_141708
Donkey polyclonal anti-rabbit alexa 594	Invitrogen	Cat#A21207; RRID: AB_141637
Goat polyclonal anti-mouse alexa 647	Invitrogen	Cat#A31625
Goat Polyclonal anti-rabbit Alexa Fluor 488	Invitrogen	Cat#A27034; RRID: AB_2536097
Chemicals, Peptides, and Recombinant Proteins		
Blue fluorescent polymer microspheres	Duke Scientific Corp.	B500
CTB alexa 555 (CTB 555)	Invitrogen	C34776
Red retrobeads	Lumafluor	N/A
Peptide: CISSWESHKSGGETRL (C terminus of Rabies G)	Eurogentec, Belgium	N/A
Peptide: TTTFKRKHFRPTPDAC (N terminus of Rabies G)	Eurogentec, Belgium	N/A
Strepavidin conjugated to Alexa Fluor 405	Invitrogen	S32351
RabiesΔG-mCherry	This paper	N/A
RabiesΔG-GFP	This paper	N/A
RabiesΔG-mCherry-EnVA	This paper	N/A
RabiesΔG-GFP-EnVA	This paper	N/A
RabiesΔG-ArchT-GFP	This paper	N/A
CAV-Cre	Kremer E., University of Montpellier, France; Soudais et al., 2001.	N/A
HSV-EF1α-Cre-Venus	BioVex (London, UK)	N/A
HSV-EF1α-GFP	BioVex (London, UK)	N/A
AAV2/9-CMV-Cre	Penn Vector Core	N/A
AAV2/7-EF1α-DIO-G	Penn Vector Core	N/A
AAV2/9-EF1α-DIO-eNpHR3.0-EYFP	Penn Vector Core	N/A
AAV2/1-CAG-DIO-GFP	Penn Vector Core	N/A
AAV2/5-EF1a-DIO-ChR2-EYFP	Penn Vector Core	N/A
AAV2/5-CaMKII-GCaMP6f	Penn Vector Core	N/A
AAV2/7-EF1α-DIO-TVA-2a-G	Roska B., FMI, Basel; Yonehara et al., 2013.	N/A
TTX	Latoxan, Valence, France	L8503
CNQX	Tocris Bioscience, Bristol, UK	1045
R-CPP	Tocris Bioscience, Bristol, UK	0247
QX-314	Tocris Bioscience, Bristol, UK	2313
Picrotoxin	Sigma-Aldrich	P1675
Fetal bovine serum (FBS)	Hyclone	SH30070.03

(*Continued on next page*)

Continued

REAGENT or RESOURCE	SOURCE	IDENTIFIER
Critical Commercial Assays		
Rapid DNA Ligation Kit	Roche	11 635 379 001
Plasmid DNA Purification	MACHEREY-NAGEL	N/A
Endotoxin-free Plasmid DNA Purification	MACHEREY-NAGEL	N/A
In-Fusion HD cloning kit	Clontech	639649
Experimental Models: Cell Lines		
B7GG	Callaway E., Salk Institute	N/A
BHK-EnVA	Callaway E., Salk Institute	N/A
HEK293-TVA	Young J., Salk Institute	N/A
HEK293T	Callaway E., Salk Institute	N/A
Experimental Models: Organisms/Strains		
C57BL6/J	Harlan Ltd	N/A
hCAR (transgenic expression of a truncated human receptor for CAV-Cre)	Pettersson, S., Karolinska Institutet, Tallone et al., 2001	N/A
LSL-R26$^{Tva\text{-}lacZ}$ (Rosa-LSL-TVA, Cre-dependent TVA expression)	Saur, D., Technische Universitat Munchen, Seidler et al., 2008	N/A
GAD2^{Cre}	Huang, Z. J., Cold Spring Harbor Laboratory, Taniguchi et al., 2011	N/A
GAD2^{Cre}::LSL-R26$^{Tva\text{-}lacZ}$ (GAD2-Cre-TVA)	This paper	N/A
C57BL6/J::hCAR (F1)	This paper	N/A
Recombinant DNA		
pSADΔG-ArchT-GFP	This paper	N/A
pAAV-EF1α-DIO-rabG	This paper	N/A
pcDNA-B19N	Callaway E., Salk Institute	N/A
pcDNA-B19P	Callaway E., Salk Institute	N/A
pcDNA-B19L	Callaway E., Salk Institute	N/A
pcDNA-B19G	Callaway E., Salk Institute	N/A
pSADΔG-F3	Callaway E., Salk Institute	N/A
Sequence-Based Reagents		
NheI-covering forward primer for Rabies G (GGCCAA GCTAGCATGGTTCCTCAGGCTCTCCTGT)	Sigma-Aldrich	N/A
AscI-covering reverse primer for Rabies G (TTAAGG CGCGCCTTACAGTCTGGTCTCACCCCC)	Sigma-Aldrich	N/A
Software and Algorithms		
ImageJ	NIH	https://imagej.nih.gov/ij/
Fiji 1.48		http://fiji.sc/
TrackEM plugin in Fiji 1.48	Cardona A. and Saalfeld S.	http://imagej.net/TrakEM2
Turboreg plugin in ImageJ	Thévenaz et al., 1998	N/A
GraphPad Prism	GraphPad Software Inc	http://www.graphpad.com/scientific-software/prism/
Imaris 7.3.1	Bitplane	www.bitplane.com/imaris/imaris
MATLAB	The MathWorks, Inc.	http://ch.mathworks.com/products/matlab
IGOR Pro	WaveMetrics	https://www.wavemetrics.com/
Neuromatic plug-in for IGOR Pro	Jason Rothman	https://www.neuromatic.thinkrandom.com
Zen softwares	Zeiss	http://www.zeiss.com/corporate/en_de/global/home.html
pClamp 10	Axon instruments	https://www.moleculardevices.com/

(*Continued on next page*)

Continued

REAGENT or RESOURCE	SOURCE	IDENTIFIER
Other		
Optic fibers	Thorlabs	BFH48-200
Custom built optrode	Lüthi A., FMI, Basel; Wolff et al., 2014	N/A
Miniature epifluorescence microscope	Inscopix	nVista HD, version 2
Gradient index lens	Inscopix	GLP-0673
Blue (465 nm, 10 mW) and yellow (590 nm, 2.5 mW) LED with LED-driver LD-1	Plexon	N/A
Yellow laser (589 nm wavelength)	CNI Lasers, China	MBL589

CONTACT FOR REAGENT AND RESOURCE SHARING

Further information and requests for reagents may be directed and will be fulfilled by the corresponding author Andreas Lüthi (andreas.luthi@fmi.ch).

EXPERIMENTAL MODEL AND SUBJECT DETAILS

Animals

Animals were individually housed under a 12 hr light / dark cycle and provided with food and water ad libitum. All animal procedures were performed in accordance with institutional guidelines and were approved by the Veterinary Department of the Canton of Basel-Stadt. For anatomical tracing, wild-type C57BL6/J (Harlan Ltd), *hCAR* (transgenic expression of a truncated human receptor for CAV-Cre) (Tallone et al., 2001), *GAD2*^{Cre} (Taniguchi et al., 2011) and *LSL-R26*$^{Tva\text{-}lacZ}$ (Rosa-LSL-TVA, Cre-dependent TVA expression) (Seidler et al., 2008) mice at an age of 2 – 6 months were used. *GAD2*^{Cre} and *LSL-R26*$^{Tva\text{-}lacZ}$ mice were crossed to generate *GAD2*-^{Cre}::*LSL-R26*$^{Tva\text{-}lacZ}$ (GAD2-Cre-TVA) mice. For behavioral experiments, 2 – 3 months old male heterozygous *hCAR* mice were used. The *hCAR* animals were F1 crossbred between wild-type C57BL6/J and homozygous *hCAR* mice. Animals were habituated to the experimenter by handling for at least 3 times before behavioral experiments. Behavioral experiments were conducted during the animal's light cycle.

Cell Culture

B7GG, BHK-EnVA, HEK293-TVA and HEK293T cells were cultured in DMEM media supported by fetal bovine serum (FBS, Hyclone) in a humidified atmosphere of 5% CO_2 and 95% air at 37°C (Osakada and Callaway, 2013). The cells were grown in 10% FBS and maintained in 2% FBS once they reached 60%–70% confluency.

METHOD DETAILS

Virus preparations

The SADΔG rabies virus was generated as described before (Osakada and Callaway, 2013). In brief, rabiesΔG-mCherry and rabiesΔG-GFP viruses were amplified from local viral stocks in B7GG cells (Baby hamster kidney cells expressing T7 RNA polymerase, rabG and histone-tagged GFP). EnvA pseudotyped rabies was generated in BHK-EnVA cells. The virus was concentrated by two rounds of centrifugation, suspended in Hank's Balanced Salt Solution (GIBCO) and titered in HEK293-TVA cells (kindly provided by J. A. T. Young, Salk Institute) with serial dilutions of the virus. The titers of the rabiesΔG-mCherry, rabiesΔG-GFP, rabiesΔG-mCherry-EnVA and rabiesΔG-GFP-EnVA were in the range of 10^8 – 10^9 infectious units/mL. Virus was stored at −80°C until further use.

Generation of RabiesΔG-ArchT-GFP virus

The coding sequence of ArchT-GFP was amplified by PCR with high-fidelity Phusion polymerase (Han et al., 2011). The PCR fragment was inserted into the pSADΔG-F3 by using the In-Fusion system (Clonetech). The resulting pSADΔG-ArchT-GFP plasmid was sequenced before virus production. G-deleted rabies virus expressing ArchT-GFP (RabiesΔG-ArchT-GFP) was recovered by transfecting B7GG cells with pcDNA-B19N, pcDNA-B19P, pcDNA-B19L, pcDNA-B19G and pSADΔG-ArchT-GFP in a humidified atmosphere of 5% CO_2 and 95% air at 35°C. The recovered RabiesΔG-ArchT-GFP was amplified in B7GG cells, concentrated by two rounds of centrifugation, and tittered in HEK293T cells. The titer of the RabiesΔG-ArchT-GFP virus was in the range of 10^7 – 10^8 infectious units/mL. Virus was stored at −80°C until use for brain injections.

Generation of AAV-DIO-G

The DNA sequence for rabies glycoprotein was amplified by PCR from pHCMV-RabG (Sena-Esteves et al., 2004) using NheI-covering forward primer (GGCCAAGCTAGCATGGTTCCTCAGGCTCTCCTGT) and AscI-covering reverse primer

(TTAAGGCGCGCCTTACAGTCTGGTCTCACCCCC). The plasmid pAAV-EF1α-DIO-rabG (AAV-DIO-G) was constructed by replacing the hChR2 sequence of pAAV-EF1α-DIO-hChR2(H134R)-EYFP (provided by K. Deisseroth, Stanford University) with the sequence for rabies glycoprotein using NheI and AscI restriction sites. Finally, the plasmid was sequenced and sent to Penn Vector Core for producing AAV2/7-EF1α-DIO-rabG (AAV-DIO-G; titer: $5.6x10^{12}$ GC/mL).

CAV-Cre virus was kindly provided by E. Kremer (University of Montpellier, France)(Soudais et al., 2001). The titer was $3.1x10^{12}$ pp/mL. HSV viruses were produced at BioVex (London, UK). The titer was in the range of 10^8 – 10^9 pp/mL (Senn et al., 2014).

Stereotaxic injections

Mice were anaesthetized with isoflurane (Attane, Provet; induction 5%, maintenance 2%) in oxygen-enriched air (Oxymat 3, Weinmann) and fixed in a stereotactic frame (Kopf Instruments). Before the surgery, systemic (Metacam, Boehringer Ingelheim) and local analgetics (Naropin, AstraZeneca AG) were administered. A feedback-controlled heating pad (FHC) was used to maintain the body temperature at 35°C. Glass pipettes (tip diameter 10 – 20 μm) connected to a Picospritzer III (Parker Hannifin Corporation) were filled with virus solutions and injected at following coordinates (posterior to Bregma, AP; lateral to the midline, LAT; below the brain surface, DV; in mm): BA: AP −1.3, LAT ± 3.5, DV −4.3; CEA: AP −1.2, LAT ± 3.0, DV −4.35; vlPAG: AP −4.8, LAT ± 0.6, DV −2.35; vHC: AP −3.5, LAT ± 3.5, DV −3.7, NST: AP −6.5, LAT ± 0.6, DV −3.75. To identify the injection site, the virus solution was typically mixed at 1:1000 with blue fluorescent polymer microspheres (Duke Scientific Corp.).

Rabies tracing

For one-step rabies tracing from vlPAG, 400 nL of rabiesΔG-mCherry were injected into vlPAG. For two-step tracing from vlPAG, a mixture (500 nL) of rabiesΔG-mCherry and HSV-Cre-Venus (ratio 3:2) were injected into vlPAG. 200 nL AAV-DIO-G were injected into CEA. In control injections for two-step tracing from vlPAG, one of these three viruses (HSV-Cre-Venus, rabiesΔG-mCherry and AAV-DIO-G) was omitted for injections.

Slice electrophysiology

300 nL CAV-Cre were injected into CEA and 200 nL AAV2/5-EF1α-DIO-ChR2-EYFP (Penn vector core) were injected into vHC. Four weeks later, 200 nL diluted red Retrobeads (Lumafluor; dialyzed against a 0.32 M sucrose solution to minimize osmotic stress in brain tissue) (Senn et al., 2014) were injected into vlPAG. One week later, acute brain slices were prepared from injected animals.

Dual-colour retrograde tracing from CEA and BA

Two different sets of injections were used. One set of injections was done in GAD2-Cre-TVA mice; a mixture (500 nL) of rabiesΔG-mCherry-EnVA and AAV-DIO-G (3:2) were injected into CEA and 200 nL HSV-GFP were injected into BA. The other set of injections was done in Rosa-LSL-TV mice; a mixture (400 nL) of AAV2/9-CMV-Cre (CMV, cytomegalovirus promoter; Penn Vector Core) and AAV-DIO-G (1:1) were injected into CEA. Two weeks later, 300 nL rabiesΔG-GFP-EnVA were injected into CEA and 200 nL CTB-555 (Invitrogen, C-34776) were injected into BA.

Rabies tracing for optogenetics

For tracing of the vHC → CEA pathway, 300 nL CAV-Cre were injected into vlPAG and 200 nL AAV2/7-DIO-G were injected into CEA. Five min later, 400 nL rabiesΔG-ArchT-GFP (ArchT group), or rabiesΔG-GFP (control group), were injected at the same coordinates. For a few animals in the control group, only rabiesΔG-GFP was injected into CEA, which can already infect vHC projection neurons. For tracing of the vHC → BA pathway, 400 nL of a mixture of AAV2/9-CMV-Cre and AAV-DIO-G (1:1) were injected into the BA. Five min later, 400 nL rabiesΔG-ArchT-GFP (ArchT group), or rabiesΔG-GFP (control group), were injected at the same coordinates. All injections were performed during a single surgery followed by bilateral implantation of optical fibers into the vHC. Behavioral experiments with optogenetic manipulations were performed 9-11 days after injections.

AAV tracing for optogenetics

For tracing of vHC → CEA axons, 300 nL CAV-Cre were injected into CEA. AAV2/9-EF1α-DIO-eNpHR3.0-EYFP or AAV2/1-CAG-DIO-GFP (Penn vector core) were injected into vHC (DV 3.6, 3.1 and 2.6). Three weeks later, optical fibers were bilaterally implanted above CEA (DV 3.8). Behavioral experiments with optogenetic manipulations were performed 5-7 weeks after injections.

Immunohistochemistry

Mice were transcardially perfused with phosphate buffered saline (PBS) followed by 4% paraformaldehyde (PFA) in PBS. Brains were post-fixed in PFA overnight at 4°C. The brains were cut into 80 μm thick coronal slices with a vibratome (Leica, Germany). Free-floating sections were rinsed in PBS. Sections were then incubated in blocking solution (3% bovine serum albumin and 0.5% Triton X-100 in PBS) containing a guinea pig anti-rabies glycoprotein (rabG) antibody for 48 hr at 4°C (1:500, custom order at Eurogentec, Belgium; two peptides for N- and C-terminals of rabG were synthesized and injected into a guinea pig, finally the antibody was purified from the serum using these two peptides). Subsequently, sections were washed with PBS three times (5 min each) and incubated for 4 hr at room temperature with fluorescent goat anti-guinea pig alexa fluor 647 (Invitrogen, A-21450; 1:500) in blocking solution. Finally, immuno-labeled sections were rinsed three times with PBS, mounted on gelatin-coated slides, dehydrated and coverslipped. Other antibodies used in this study were goat anti-GFP (Abcam, ab6673, 1:500), rabbit anti-mCherry (Abcam, ab28664, 1:500), mouse anti-NeuN (Millipore, MAB377, 1:500), rabbit anti-GABA (Sigma, A2052, 1:500) and rabbit anti-CaMKII (Abcam, ab52476, 1:500). All secondary antibodies were alexa fluor coupled (Invitrogen: donkey anti-goat alexa 488, A11055; donkey anti-rabbit alexa 488, A21206; donkey anti-rabbit alexa 594, A21207; goat anti-mouse alexa 647, A31625). Slices were imaged with a

LSM 700 confocal microscope (Zeiss, Germany). To quantify the cell number per animal, every third section was scanned and analyzed in Zen software (Zeiss, Germany).

Optogenetics and behavior

For optogenetic manipulations of behavior, optic fibers were bilaterally implanted in vHC (AP −3.5, LAT ± 3.5, DV −2.5) in the same surgery after injections of rabies vectors or implanted above CEA (AP −1.2, LAT ± 3.0, DV −3.8) three weeks after injections of AAV vectors. Optic fibers (0.48 numerical aperture, 200 μm diameter, Thorlabs) were assembled in custom-built connectors as previously described (Wolff et al., 2014) and fixed on the skull with cyanoacrylate glue (Ultra Gel, Henkel) and dental cement (Paladur, Heraeus). Implanted connectors were linked to a custom-built laser bench via optic fibers during behavior sessions with optogenetic manipulations. An AOTF (AA Opto-Electronic) was used to control laser intensity (MBL589, 589 nm wavelength, CNI Lasers, China). The laser intensity was 15 – 20 mW at end of the optic fiber.

Mice were submitted to an auditory fear conditioning paradigm. Two different contexts for conditioning (context A) and extinction (context B) were used. Context A and B were cleaned before and after each session with 70% ethanol or 1% acetic acid, respectively. Freezing behavior was quantified using an automatic infrared beam detection system (Coulbourn Instruments). The animals were considered freezing if no movement was detected for 2 s and the measure was expressed as a percentage of time spent freezing. 24 hr after fear conditioning in context A, mice were subjected to two extinction training sessions (one extinction session per day) in context B. 24 hr later, animals were tested for extinction retrieval in context B followed by test for context-dependent fear renewal in context A 2 hr later. Each behavior session consisted of a 10 min baseline prior to the first CS presentation, which gives the animal sufficient time to show normal locomotion after exposure to conditioning or extinction context. The 2 min prior to the first CS were used to measure baseline freezing. The CS consisted of 500 ms pips repeated at 1 Hz (pip frequency: 3 kHz; sound pressure level: 75 dB). Each CS was 30 s long (except 10 s for fear conditioning session). CS inter-trial intervals ranged between 35 s and 60 s. During fear conditioning, the CS was paired to the US (2 s, 0.7 mA foot shock back to back with the last CS pip; 5 CS/US pairings; inter-trial interval: 35 – 60 s). 12 CS were presented in each fear extinction session. For extinction retrieval, 4 CSs were presented. Mice showing high freezing (> 50%) to CS during extinction retrieval were considered to have deficits in extinction learning or memory and thus were excluded from the analysis. For fear renewal, one CS was presented and the entire CS was paired with 30 s constant light stimulation. Some animals were subjected to a test for CS fear retrieval instead of extinction training after auditory fear conditioning. During the CS fear retrieval test, one CS was presented with 30 s constant light stimulation.

Contextual fear conditioning paradigm took place in context A. The first 2 min in the context was used to measure the baseline freezing. In total, 5 USs were delivered (first US at 2:10 min; US: 0.7 mA, 2 s; inter-US interval: 35 - 60 s). The 10 s period before each US was used to measure inter-US freezing. The conditioning session terminated 30 s after the last US. 24 hr later, animals were tested for contextual fear retrieval in context A for 5 min with a 5 min constant light stimulation throughout the whole session.

After the end of the experiment, mice were transcardially perfused with PFA. Brains were post-fixed in PFA overnight at 4°C, cut with a Leica vibratome and imaged with AxioScan or Axioimager Z1 microscopes (Zeiss, Germany). The fiber tip positions and injection sites in the brain were mapped according to the mouse brain atlas (Paxinos and Franklin, 2001).

Slice electrophysiology

Mice were deeply anaesthetized by intraperitoneal injection of ketamine/medetomidine (250 mg/kg and 2.5 mg/kg bodyweight, respectively) and transcardially perfused with ice-cold slicing ACSF (in mM: 124 NaCl, 2.7 KCl, 26 $NaHCO_3$, 1.25 NaH_2PO_4, 2.5 glucose, 50 sucrose, 0.1 $CaCl_2$, 6 $MgCl_2$, 3 kynurenic acid, oxygenated with 95% O_2/5% CO_2, pH 7.4). The brain was rapidly removed from the skull, and coronal brain slices (300 μm) containing the CEA were prepared in ice-cold slicing ACSF with a vibrating-blade microtome (HM 650 V, Microm) equipped with a sapphire blade. Slices were maintained for 45 min at 37°C in an interface chamber containing recording ACSF (in mM: 124 NaCl, 2.7 KCl, 26 $NaHCO_3$, 1.25 NaH_2PO_4, 18.6 glucose, 2.25 ascorbic acid, 2 $CaCl_2$, 1.3 $MgCl_2$, oxygenated with 95% O_2/5% CO_2, pH 7.4) and subsequently kept at room temperature (20-22°C) until start of recordings. Slices were then transferred to a submerged recording chamber on an upright microscope (BX50WI, Olympus) and superfused with recording ACSF (as above, except: 2.5 mM $CaCl_2$, 100 μM picrotoxin) at a perfusion rate of 2-4 mL/min at 35°C. ChR2-EYFP-positive fibers from vHC and retrobead-positive CEA neurons were visualized using epifluorescence and a 40x objective (LumPlanFl 40x/0.8, Olympus). Patch electrodes (3-5 MΩ) were pulled from borosilicate glass tubing and filled with internal solution (for voltage-clamp recordings in mM: 110 CsCl, 30 K-gluconate, 1.1 EGTA, 10 HEPES, 0.1 $CaCl_2$, 4 Mg-ATP, 0.3 Na-GTP, 4 QX-314 chloride and 0.4% biocytin, pH 7.3; for current clamp recordings in mM: 130 K-gluconate, 5 KCl, 10 HEPES, 10 phosphocreatine-Na_2, 4 Mg-ATP, 0.4 Na-GTP, 0.6 EGTA and 0.4% biocytin, pH 7.25). Voltage clamp recordings were acquired in whole-cell mode at a holding potential of −70 mV. In a subset of neurons, the ability to induce action potentials in CEA cells by vHC fiber activation was first tested in on-cell mode. ChR2 expressing afferents were photostimulated using a blue LED (465 nm, with LED-driver LD-1, Plexon) connected to an optical fiber, which was positioned above the CEA. Blue light pulses of 10 mW with 10 ms duration were applied at a frequency of 1 Hz. In some slices, TTX (1 μM) and CNQX (10 μM) were administered with the recording ACSF for the last cell recorded from. Input-output curves were generated in current clamp mode by applying 25 pA current steps of 500 ms duration starting from −100 pA, while holding the cell at −70 mV. To assess the impact of vHC inputs on input-output function, the same protocol was repeated while shining blue light only during the current steps. Data were acquired with a Multiclamp 700A amplifier, Digidata 1440A A/D converter and pClamp 10 software (all Axon instruments) at 20 kHz and filtered at 4 kHz (voltage clamp) or 10 kHz (current clamp). Whole-cell

recordings were excluded if the access resistance exceeded 25 MΩ or changed more than 20% during the recordings. Data were analyzed using IGOR Pro software (Version 6.35A5, WaveMetrics) with NeuroMatic plug-in (www.neuromatic.thinkrandom.com). All cells were filled with biocytin during recording. Outside-out patches were pulled at the end of each recording and slices were fixed for 1 hr in 4% paraformaldehyde in PBS for subsequent immunohistochemistry.

To test functionality of rabiesΔG-ArchT-GFP, coronal brain slices of the vHC were prepared as described above. Whole-cell current clamp recordings (as above) from GFP-positive cells were obtained at room temperature (20-22°C) in recording ACSF (as above, except 10 μM CNQX, 10 μM CPP and 100 μM picrotoxin). An optical fiber connected to a yellow LED (590 nm, 2.5 mW, with LED-driver LD-1, Plexon) was positioned above the vHC. ArchT functionality was tested with 500 ms yellow light pulses. Moreover, a depolarising current step of 500 ms duration was applied from a holding potential of −60 mV to induce action potentials and the same current step was subsequently paired with yellow light to test for abolishment of spiking with ArchT activation.

All chemicals were purchased from Sigma-Aldrich (Buchs, Switzerland) except for CNQX, CPP and QX-314 (Tocris Bioscience, Bristol, UK) and TTX (Latoxan, Valence, France).

Immunohistochemistry

Free-floating sections were washed with PBS three times before incubation in blocking solution (3% normal goat serum, 1% bovine serum albumin (BSA) and 0.5% Triton X-100 in PBS) for 2 hr at room temperature. Slices were then incubated for 48 hr at 4°C in blocking solution with rabbit anti-GFP antibody (1:1000; Invitrogen, A11122). Sections were washed in PBS three times before adding goat anti-rabbit Alexa Fluor 488 secondary antibody (1:750, A27034) and Strepavidin conjugated to Alexa Fluor 405 (1:1000; Invitrogen, S32351) in blocking solution for 24 hr at 4°C. Finally, slices were washed in PBS four times, mounted and coverslipped, and imaged using a confocal microscope (LSM710, Carl Zeiss AG) with 63x objective and 2-fold digital zoom.

Optrode recordings of neurons infected with rabiesΔG-ArchT-GFP

A custom-built optrode was used for simultaneous optogenetic stimulations and single-unit recordings as previously described (Wolff et al., 2014). Optrodes consisted of an optic fiber connector with a recording electrode attached directly to the fiber, with the tip protruding approximately 300 – 500 μm beyond the fiber. Electrodes were made of 16 individually insulated, gold-plated nichrome wires (13 mm inner diameter, impedance 30 – 100 kV, Sandvik), attached to a connector (18 pin, Omnetics). The whole implant was fixed to the skull. 30 s yellow light was delivered into vHC to activate ArchT during single-unit recordings. Single-unit spike sorting was performed using Offline Spike Sorter (OFSS, Plexon). A recorded unit was considered to be light-sensitive if the spike number during light stimulation was significantly lower than during the 30 s period before light stimulation.

3D Reconstructions and quantitative analysis of anatomical tracings

The brains were coronally sectioned as 80 μm thick slices on a vibratome (Leica, Germany). All brain sections were collected and sorted. The brain sections were scanned by AxioScan or Axioimager Z1 (Zeiss, Germany) with a 5x objective. The original image data were exported as TIFF files. All the images for individual brain sections were sorted in correct order and aligned with the TrackEM plugin in Fiji (Fiji 1.48) and then exported into Imaris software (Imaris 7.3.1) for analysis. The contours for different brain structures were drawn in Imaris. The cell bodies in a brain structure were semi-automatically detected as spots in Imaris (automate detection first and then manual verification). Finally, the spot coordinates in the brain were exported into MATLAB from Imaris by the Imaris XTensions (7.3.1) and their 3D distributions in the brain were analyzed in MATLAB. For the hippocampus, the beginning of the anterior hippocampus (Bregma −0.92 mm in mouse brain atlas by Paxinos and Franklin, 2001) was used as the reference for each brain sample. For analysis of the distribution of hippocampal cells in the dorsal-ventral axis, the dorsal-ventral distance for each hippocampal section was calculated based on the contours drawn in Imaris. Next, each section was divided into 50 bins in the dorsal-ventral axis and the cell number was counted in each bin. Finally, the cell numbers were normalized by the total number of rabies-labeled neurons in hippocampus. In the end, these normalized cell numbers were averaged across different brain samples. These normalized cell numbers were represented by color-coded density map or density-based contour plot (Figure S3C). Another way to look at the cell distribution are density maps for individual sections. For each section, a sliding window (200 μm square window) is used to calculate the cell density and the sliding step is 100 μm (Figure S1E).

Microendoscope imaging

500 nl of AAV2/5-CaMKII-GCaMP6f vectors (Penn Vector Core, Titer: $1.31x10^{13}$ GC/mL) were injected in vHC (AP −3.5 mm; LAT 3.5; DV, 3.7, 3.2, and 2.7, multiple injections). One week after AAV injection a gradient index lens microendoscope (GLP-0673, Inscopix) was implanted in the vHC (AP −3.4, LAT −3.3, DV 3.3) during a second surgery. Briefly, a small craniotomy was made above the vHC and an incision above the imaging cite was made using a sterile needle. The microendoscope was lowered into the brain using a precision microdrive and fixed to the skull using UV light-curable glue (Henkel, Loctite 4305). A custom made head bar was glued to the skull for animal fixation during the miniature microscope mounting procedure. Finally, dental acrylic was used to seal the skull. One week after microendoscope implantation, we started to check for GCaMP6f fluorescence using a miniature epifluorescence microscope (Inscopix, nVista HD, version 2). Once sufficient expression was determined, we fixed the microscope via a baseplate (Inscopix) to the skull using light curable glue (Vertise Flow, Kerr, ABCDental) under brief isoflurane anesthesia. The microscope was detached, the baseplate sealed with a base plate cover (Inscopix) and the mouse returned to its home cage. Imaging experiments

were performed five weeks after virus expression. Mice were habituated to the miniature microscope mounting procedure for three consecutive days before the start of the experiment. The microscope was mounted on a daily basis right before the behavioral session. Fear conditioning, extinction, extinction test and fear renewal experiments were performed similarly to the optogenetic experiments in Figure 6A. Cell health was checked under anesthesia after the behavioral experiments with two-photon microscopy via the GRIN lens using a FluoView two-photon microscope (Olympus, Japan) in conjunction with a 16X Nikon objective. Miniature microscope imaging data were acquired using the nVista software (Inscopix) with the following settings: field of view: 614 × 614 μm; Gain: 1, LED Power: 30 - 40%. Imaging frames were normalized across the whole frame by diving each frame by a Fast Fourier Transform band pass-filtered version of the frame (ImageJ). XY movement was corrected using the "Turboreg" plugin in ImageJ (Thévenaz et al., 1998). Spatial filters for individual neurons were identified using principal and independent component analysis as described previously (Mukamel et al., 2009). Next, we applied these filters to the movie to obtain raw Ca^{2+} fluorescence. Spatial filters that did not correspond to neurons (e.g., blood vessels) were discarded. Relative changes in Ca^{2+} fluorescence were calculated by $\Delta F/F_0 = (F - F_0)/F_0$ (F_0 = mean fluorescence of entire trace). Cells were registered across sessions based on cell maps generated by a projection of all cell filters onto one plane. The extinction test session was used as a reference map and the renewal session cell map was aligned using TurboReg. Image analysis was performed in MATLAB (MathWorks) and statistical analysis was based on Wilcoxon signed-rank test of average time-binned Ca^{2+} signals to identify context-responsive cells and paired Wilcoxon signed-rank test with post hoc Benjamini-Hochberg correction for repeated tests to identify significant bins (Figure S4G) using MATLAB and R (www.r-project.org).

QUANTIFICATION AND STATISTICAL ANALYSIS

Mean values are accompanied by SEM. No statistical methods were used to predetermine sample sizes. Data collection and analysis were not performed blind to the conditions of the experiments. Statistical analysis was performed in GraphPad Prism 6 and R. Paired t test, one-way ANOVA test, Mann-Whitney U test and Wilcoxon matched-pairs signed rank test were used to test for statistical significance when appropriate. Statistical parameters including the exact value of n, precision measures (mean ± SEM) and statistical significance are reported in the text and in the figure legends (see individual sections). The significance threshold was placed at $\alpha = 0.05$ (n.s., $p > 0.05$; *, $p < 0.05$; **, $p < 0.01$; ***, $p < 0.001$; ****, $p < 0.0001$).

Supplemental Figures

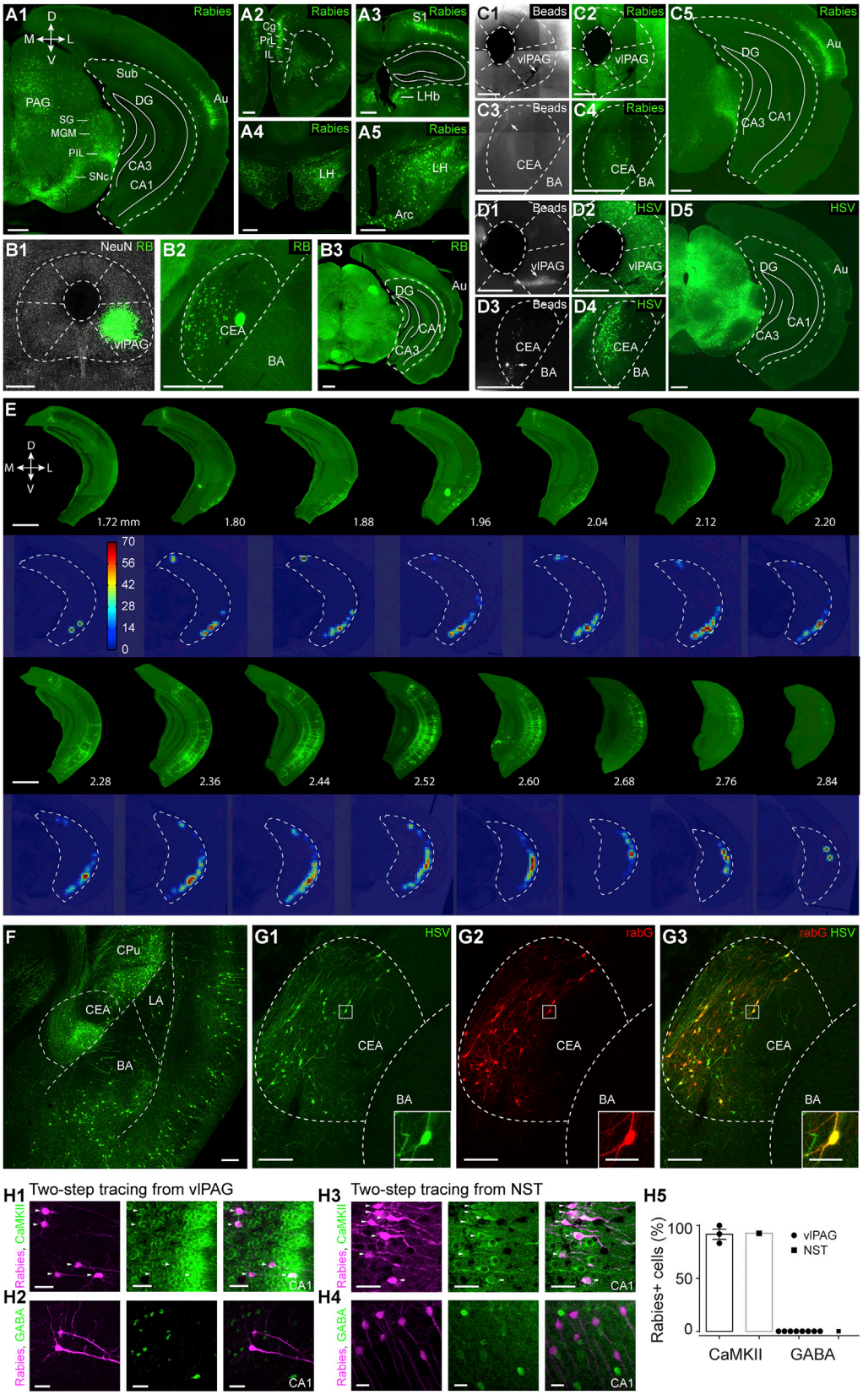

(legend on next page)

Figure S1. Related to Figures 1 and 2

(A–D) Non *trans*-synaptic rabies tracing from vlPAG. Scale bars, 0.5 mm.

(A1–A5) Examples showing rabiesΔG-mCherry-labeled cells in various brain areas (in addition to CEA shown in Figure 1B) by non *trans*-synaptic retrograde rabies tracing from vlPAG (local injection of rabiesΔG-mCherry and beads into vlPAG).

(B1–B3) Examples showing local injections of retrobeads (RB) into vlPAG (B1) and bead-labeled cells in CEA (B2) other brain areas (B3). Consistent with non *trans*-synaptic rabies tracing (A1), no cells in vHC were labeled (B3).

(C1–C5) Examples showing local injections of rabiesΔG-mCherry and beads (arrow) into vlPAG (C1 – C2), AAV-DIO-G and beads into CEA (C3, arrow) and rabies-labeled cells in CEA (C4) and other brain areas (C5). No cells in vHC were labeled.

(D1–D5) Examples showing local injections of HSV-Cre-Venus and beads (arrow) into vlPAG (D1 – D2), AAV-DIO-G and beads into CEA (D3, arrow) and HSV-labeled cells in CEA (D4) and other brain areas (D5). No cells in vHC were labeled.

Abbreviations: vlPAG, ventrolateral periaqueductal gray; SG, suprageniculate thalamic nucleus; MGM, medial geniculate nucleus, medial part; PIL, posterior intralaminar thalamic nucleus; SNc, substantia nigra, pars compacta; DG, dentate gyrus; CA3, field CA3 of hippocampus; CA1, field CA1 of hippocampus; Au, auditory cortex; Cg, cingulate cortex; PrL, prelimbic cortex; IL, infralimbic cortex; S1, primary somatosensory cortex; LHb, lateral habenular nucleus; LH, lateral hypothalamic area; Arc, arcuate hypothalamic nucleus. M: median; L: lateral; D: dorsal; V: ventral.

(E) Example pictures showing vHC cells labeled by *trans*-synaptic rabies tracing from vlPAG-projecting CEA output neurons. Consecutive coronal sections are sorted from anterior to posterior coordinates. Each section is 80 μm thick and its relative distance to the anterior tip of the dorsal hippocampus (Bregma −0.94 mm) is indicated. The corresponding cell density map is shown below each section. Scale bars, 1 mm.

(F) Example pictures showing that cells in BLA and caudate putamen (CPu) were labeled by *trans*-synaptic rabies tracing from vlPAG-projecting CEA output neurons. Scale bar, 0.1 mm.

(G1–G3) To validate Cre-dependent expression of rabies glycoprotein (rabG), HSV-Cre-Venus was injected into vlPAG and AAV-DIO-G was injected into CEA. Examples pictures showing HSV-Cre-Venus-labeled cells (G1) and rabG immunostaining (G2) in CEA. 97% of rabG-stained cells are co-labeled by HSV, suggesting faithful expression of rabG (G3). Insets are the magnification of boxed areas. Scale bars, 200 μm. Scale bars in insets: 50 μm.

(H) Immunohistochemical analysis of rabies-labeled cells in vHC. Scale bars, 50 μm.

(H1) Example pictures showing immunostaining for CaMKII and rabies labeling in vHC upon *trans*-synaptic tracing from vlPAG-projecting neurons in CEA. Arrows indicate co-localization of CaMKII and rabies labeling.

(H2) Example pictures showing immunostaining for GABA and rabies labeling in vHC upon *trans*-synaptic retrograde tracing from vlPAG-projecting neurons in CEA.

(H3) Examples of immunostaining for CaMKII and rabies labeling in vHC upon *trans*-synaptic retrograde tracing from CEA output neurons targeting the nucleus of the solitary tract (NST). Arrows indicate co-localization of CaMKII and rabies labeling.

(H4) Example pictures showing immunostaining for GABA and rabies labeling in vHC upon *trans*-synaptic retrograde tracing from NST-projecting neurons in CEA.

(H5) Summary plot (mean ± SEM) illustrating the percentage of rabies-labeled cells co-staining for CaMKII or GABA in the hippocampus. Two-step tracing from vlPAG: circles, CaMKII, 91.78% ± 4.81%, n = 3 animals; GABA, 0% ± 0%. n = 8 animals. Two-step tracing from NST: squares, CaMKII, 92.59%, n = 1 animal; GABA, 0%, n = 1 animal.

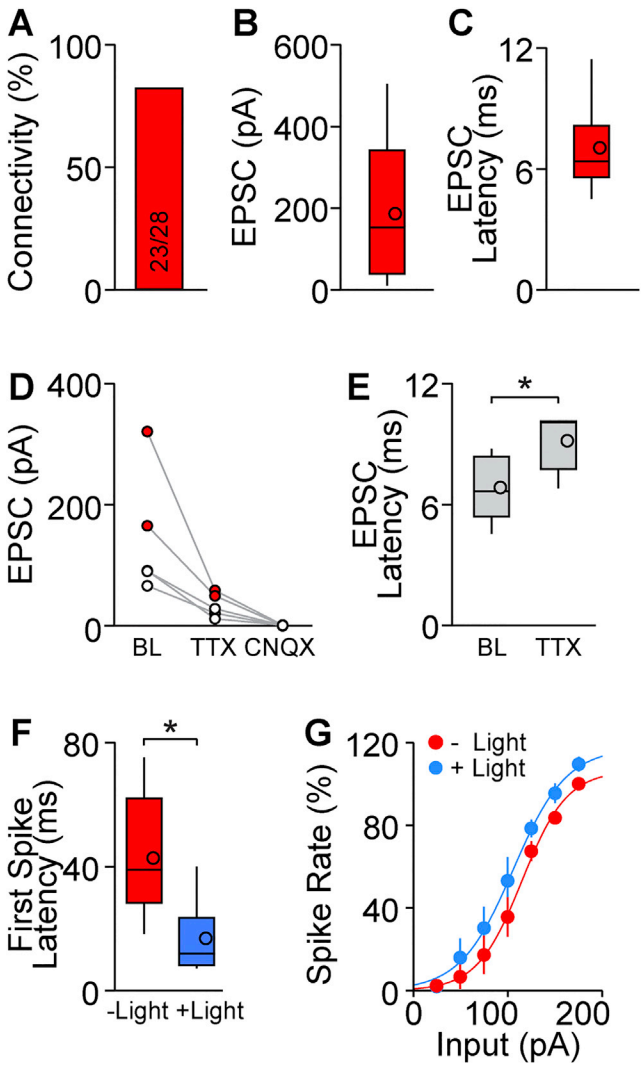

Figure S2. Recordings from RB+ Neurons in CEA, Related to Figure 3

(A) Connectivity from vHC afferents to RB+ CEA neurons was 82.1% (23 out of 28 cells).

(B and C) Summary of EPSC amplitudes and EPSC peak latencies in RB+ neurons recorded in CEA. Data are presented as median with 25/75 percentile (box) and 10-90 percentile (whiskers). The circle indicates mean; n = 14 cells.

(D) Light-evoked EPSC amplitudes recorded from CEA neurons during baseline condition (BL), bath application of TTX and CNQX. Red circles are from RB+ neurons. The normalized results are shown in Figure 3I.

(E) The EPSC peak latencies recorded from CEA neurons (same neurons as in D) during BL and bath application of TTX.

(F) Latency to the first action potential at a current injection of +100 pA is significantly shorter with vHC fiber activation. (n = 7 cells; Wilcoxon matched-pairs signed rank test, p = 0.0156).

(G) vHC fiber photostimulation increases the excitability of CEA neurons. Spike rate is normalized to the maximum frequency in baseline condition of each cell. Input-output curves are shifted to the left by −11.9 pA with vHC fiber activation (I_{half} baseline 106.1 pA, I_{half} light 94.3 pA; paired t test, p = 0.0697; n = 7 cells). Data are presented as mean ± SEM, n = 7 cells.

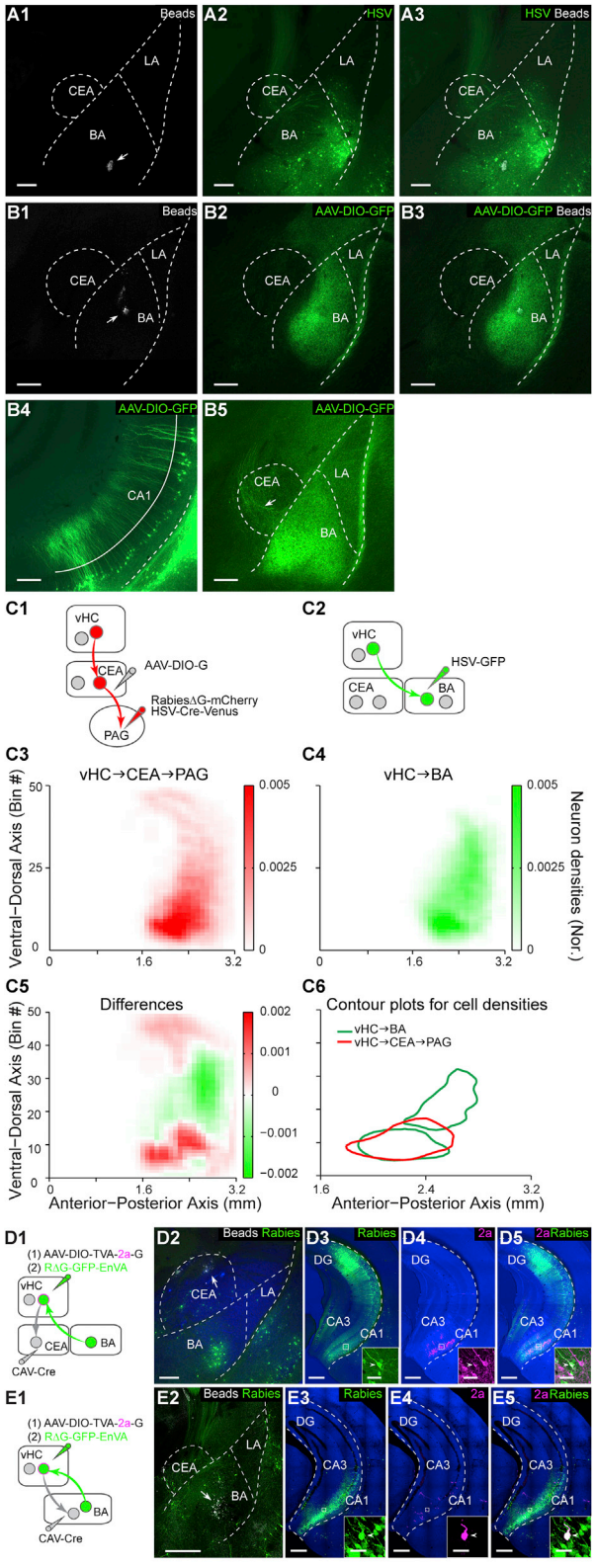

Xu et al. Figure S3

(legend on next page)

Figure S3. Related to Figure 4

(A and B) En-passant BA-projecting axons in CEA. Scale bars, 200 μm.

(A1–A3) Example pictures showing BA-projecting axons passing through CEA. The retrograde axon tracing from BA was done by co-injection of blue beads (A1, arrow) and HSV-GFP (A2) in BA. The overlay is shown in (A3).

(B1–B5) Example pictures showing BA-projecting axons passing through CEA (B5, arrow). The BA-projecting axons from vHC were labeled by co-injection of blue beads (B1, arrow) and CAV-Cre (canine adenovirus type 2 expressing Cre-recombinase) into BA (B2 and B3) and AAV2/1-CAG-DIO-GFP into vHC (B4).

(C) Spatial distribution of CEA- and BA-projecting neurons in hippocampus.

(C1 and C2) Scheme illustrating the experimental design used for retrograde tracing of the vHC → CEA pathway (C1) and the vHC → BA pathway (C2).

(C3 and C4) Density maps for CEA-projecting and BA-projecting vHC neurons along the anterior-posterior hippocampal axis. Each coronal section of hippocampus is divided into 50 bins along the ventral-dorsal axis (y axis) of the hippocampus. Cell numbers in each bin were normalized to the total number of vHC neurons labeled in each brain sample and were color-coded to reflect cell density. Density maps were averaged across different animals (vHC → CEA pathway, 92% ± 1% in CA1 and 8% ± 1% in Subiculum; n = 8; vHC → BA pathway, 95% ± 1% in CA1; 5% ± 1% in Subiculum; n = 5; Mann Whitney U test for ratios of CA1 neurons between two pathways, p = 0.09). No cells were labeled in dorsal HC.

(C5) Plot illustrating difference (C3 minus C4) between density maps shown in (C3) and (C4). vHC neurons projecting to CEA are located more ventrally than BA-projecting neurons.

(C6) Contour plots displaying isolines based on highest density in maps shown in (C3) and (C4).

(D and E) *Trans*-synaptic rabies tracing from BA- or CEA-projecting vHC neurons.

(D1) Injection scheme illustrating experimental design for *trans*-synaptic retrograde tracing from vHC neurons projecting to CEA. CAV-Cre and beads were co-injected into CEA and AAV-DIO-TVA-2a-G is injected into vHC for Cre-dependent expression of TVA, G (glycoprotein) and the 2a tag (Yonehara et al., 2013). Two weeks later, RabiesΔG-GFP-EnVA was injected into vHC.

(D2) Example picture illustrating labeling in the BA after *trans*-synaptic rabies tracing from CEA-projecting vHC neurons (342 and 186 cells, n = 2 animal). The injection site in CEA is indicated by beads (arrow).

(D3–D5) Example pictures showing rabies-labeled cells (green) and 2a immunostaining (magenta, rabbit anti-2a, Millipore ABS31, 1:500; Donkey anti-Rabbit 647, Invitrogen A31573, 1:500) in vHC. Blue background is the transmission image. Insets are magnifications of the boxed area in which a starter cell (arrow) was identified.

(E1) Injection scheme illustrating experimental design for *trans*-synaptic retrograde tracing from vHC neurons projecting to BA. CAV-Cre and beads are co-injected into BA and AAV-DIO-TVA-2a-G is injected into vHC. Two weeks later, RabiesΔG-GFP-EnVA is injected into vHC.

(E2) Example picture illustrating sparse labeling in the BA after *trans*-synaptic rabies tracing from BA-projecting vHC neurons (65 ± 35 cells, n = 4 animals). The injection site in the BA is indicated by beads (arrow).

(E3–E5) Example pictures showing rabies-labeled cells and 2a immunostaining in vHC. Insets are magnifications of the boxed area in which a starter cell (arrow) was identified.

Scale bars, 0.5 mm; insets, 0.02 mm.

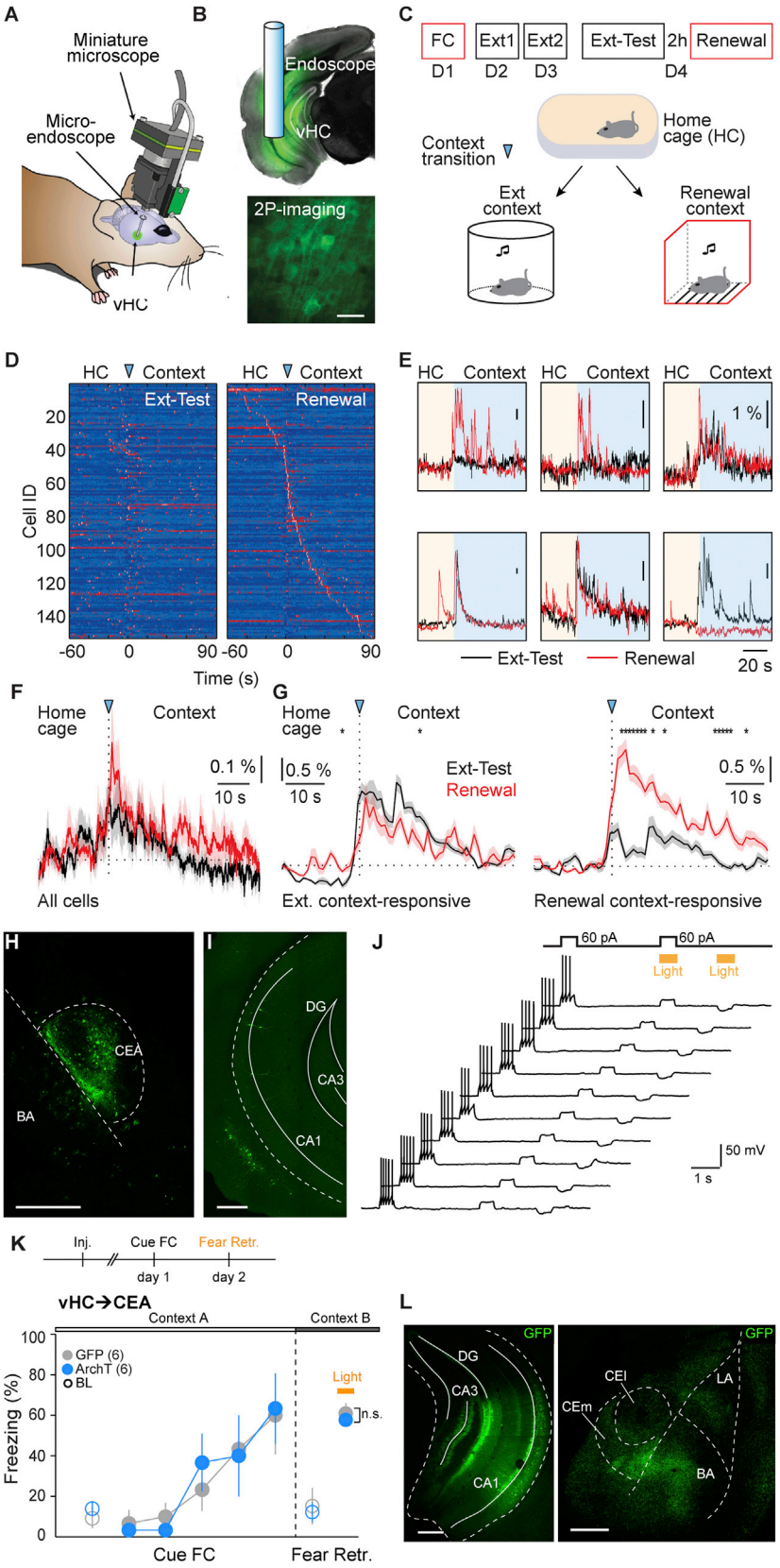

(legend on next page)

Figure S4. Related to Figures 5 and 6

(A–G) Deep brain Ca^{2+} imaging of vHC activity upon home cage to context transition.

(A) Scheme showing combined miniature microscope and endoscope imaging of vHC in freely moving animals.

(B) Top, AAV2/5-CaMKII-GCaMP6f expression and microendoscope (GRIN) lens position in vHC. Bottom, two-photon microscopy in vivo image of GCaMP6f-expressing neurons in vHC via the GRIN lens. Scale bar, 20 μm.

(C) Experimental paradigm to measure context activation of vHC. Animals were trained with a similar fear renewal paradigm as shown in Figure 6A. vHC activity was analyzed on Day 4 upon context transition from home cage (HC) to extinction test context or HC to renewal context.

(D) Normalized population activity before and after context transition for extinction test and renewal (session-to-session matched neurons, n = 153 out of 3 animals). Cells were sorted based on the timing of peak Ca^{2+} fluorescence during renewal, demonstrating a context-specific temporal ensemble pattern in vHC. Time 0 s (blue triangle) indicates the time point at which the animal first touches the context.

(E) Ca^{2+} traces of six example neurons upon the context transition from HC to the extinction test context (black) and from HC to the renewal context (red).

(F) Averaged population response of session-matched cells (same as in D) upon context transition.

(G) Population Ca^{2+} responses (mean ± SEM, 1 s time bin) of context-responsive neurons before and after context transition. Context-responsive neurons were defined by a significantly increased mean Ca^{2+} response before and after context transition (1 s bins, 60 s before versus after context transition; Wilcoxon signed-rank test). Left: On average, extinction context-responsive neurons show similar context transition-evoked Ca^{2+} responses in the renewal context compared to the extinction context (n = 45 cells, 30% ± 2% activated neurons/animal, N = 3). Right: Renewal context-responsive neurons show larger Ca^{2+} responses upon the transition in the renewal context compared to the extinction context (n = 50 cells, 38% ± 9% activated neurons/animal, N = 3). Significance is determined by paired Wilcoxon signed-rank test with Benjamini-Hochberg correction for repeated-measures; * = $p < 0.05$.

(H and I) Examples of rabiesΔG-ArchT-GFP infections in CEA (A) and vHC (B) after local injection into CEA. RabiesΔG-ArchT-GFP infects local neurons in CEA, but very few neurons in vHC. Scale bars, 400 μm.

(J) Top, scheme showing the whole-cell recording protocol and light stimulation. Bottom, raw traces of whole-cell recording for the example recording shown in Figure 5B. Three tests were performed in each trial. The first test is that the current injection (−60 pA) evoked a train of spikes, the second test is that the current-evoked spikes were reliably inhibited by light stimulation, and the last test is that the light stimulation only elicited hyperpolarization.

(K) vHC→CEA pathway is not necessary for the retrieval of non-extinguished CS fear. Top, scheme illustrating the behavioral paradigm used to test the functional role of the vHC→CEA pathway in the retrieval of non-extinguished CS fear. During the fear retrieval session (Fear Retr.), the entire CS (tone) was paired with yellow light stimulation (yellow bar) targeted to the vHC. Bottom, summary data (mean ± SEM) of CS-induced freezing during tone fear conditioning (Cue FC) and subsequent CS fear retrieval (Fear Retr.). Freezing in all sessions is shown for single CSs. Open circles indicate 2 min baseline (BL) freezing for each behavioral session. Inhibition of the vHC→CEA pathway does not affect CS fear retrieval without extinction (control, gray; 62.2% ± 5.1%, n = 6; ArchT, blue; 58.9% ± 3.2%, n = 6; Mann-Whitney U test, $p = 0.426$).

(L) vHC axonal distribution in amygdala. Left, example picture showing AAV2/9-CMV-GFP injection in vHC. Right, example picture showing axonal tracings in amygdala. Scale bars, 400 μm.

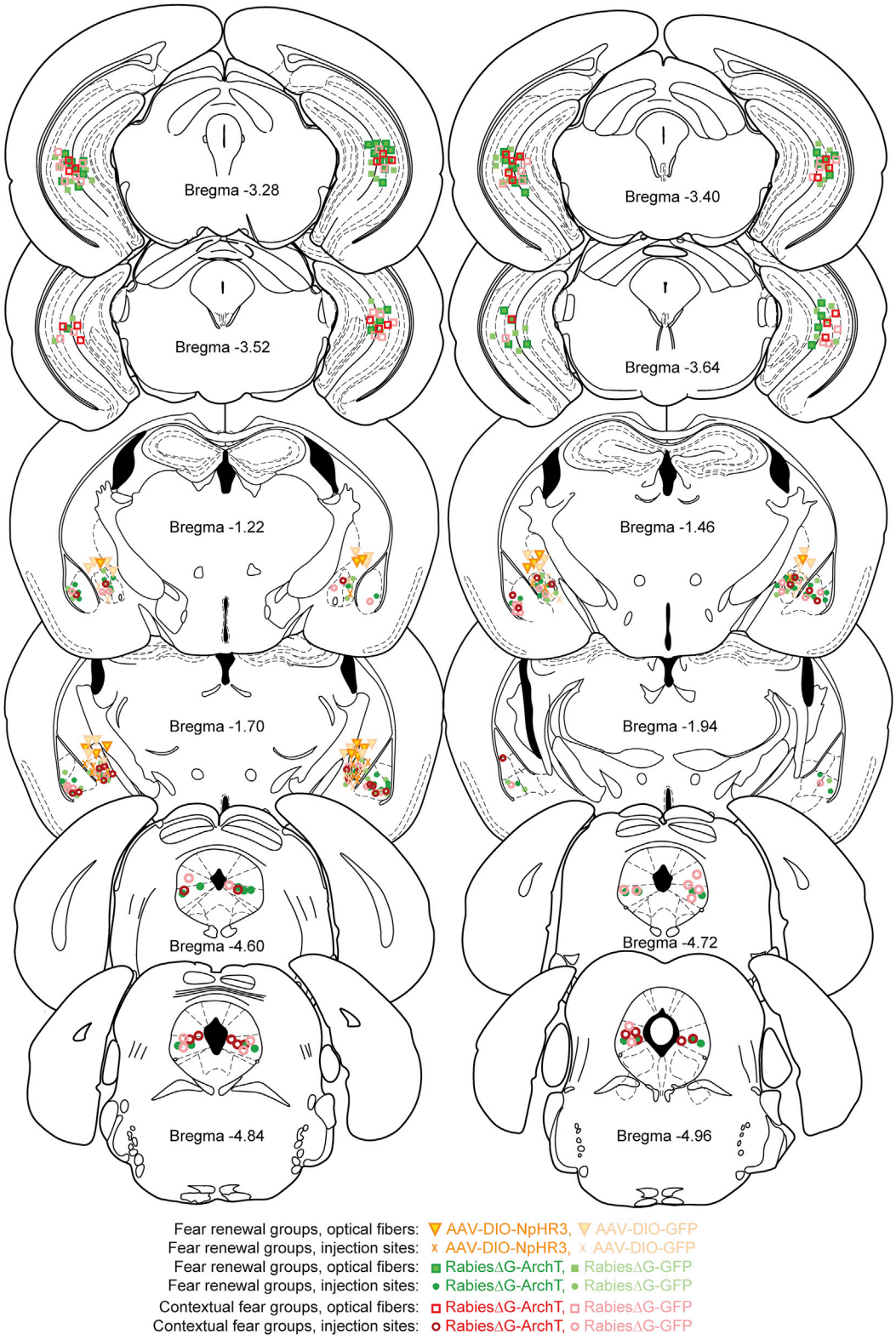

Figure S5. Optical Fiber Placements and Injection Sites for Behavioral Experiments, Related to Figures 5 and 6

Positions of implanted optical fiber tips (squares and triangles) and injection sites (circles and crosses) in animals with optogenetic manipulations during fear renewal are shown in green and yellow, and those in animals with optogenetic manipulations during contextual fear retrieval are shown in red.

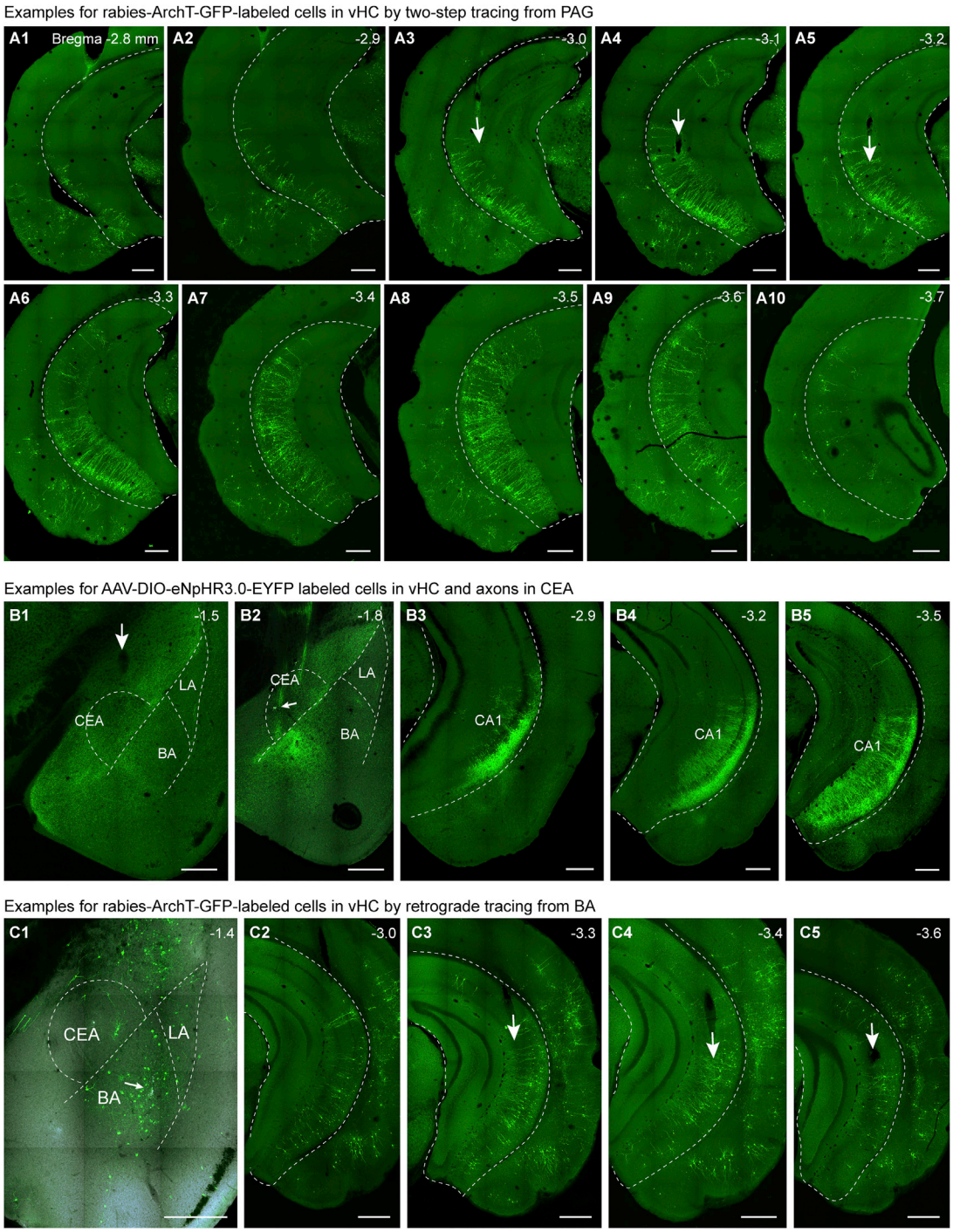

Figure S6. Histology Examples for Behavior Experiments with Optogenetics, Related to Figures 5 and 6

(A1–A10) Examples for vHC cells labeled by rabiesΔG-ArchT-GFP after transsynaptic tracing from PAG-projecting CEA neurons. The arrows indicate optical fiber tracks. Unlike rabiesΔG-mCherry and rabiesΔG-GFP, rabiesΔG-ArchT-GFP primarily label vHC neurons but very few APir neurons (also see C1 – C5).

(B1–B5) Examples for eNpHR3.0-EYFP labeled cells in vHC and axons in CEA. The arrow in B1 indicates optical fiber track. The CAV-Cre and blue beads were co-injected into CEA (arrow in B2, beads shown in gray). Scale bars, 0.5 mm.

(C1–C5) Examples for vHC cells labeled by rabiesΔG-ArchT-GFP after transsynaptic tracing from the BA. The arrow in C1 indicates co-injected beads (gray). The arrows in C3 – C5 indicate optical fiber tracks.